FOURTEEN

Modern Andean rainfall variation during ENSO cycles and its impact on the Amazon drainage basin

Bodo Bookhagen[1] and Manfred R. Strecker[2]

[1]*UC Santa Barbara, California, USA*
[2]*Universität Potsdam, Germany*

Abstract

The modern and past spatiotemporal rainfall variation in South America is strongly controlled by El Niño-Southern Oscillation (ENSO) cycles. Generally, rainfall during positive ENSO anomalies (El Niño) is increased in parts of the west coast of South America, while negative ENSO anomalies (La Niña) increase rainfall in parts of central South America and in the Amazon drainage basin, although the precise spatiotemporal rainfall pattern is complex. As rainfall modulates discharge and erosion processes, the global-scale ENSO phenomenon thus strongly controls sediment flux and aggradation/deposition cycles in the Andes and in the adjacent lowlands. However, the spatiotemporal magnitude variation in rainfall and discharge between contrasting ENSO cycles remains weakly constrained, as there are only a limited number of rain- and river-gauge networks in the remote areas of the Andes and Amazon drainage basin. Here, we exploit calibrated remote-sensing data to characterize rainfall and discharge variations of the Amazon drainage basin at a high temporal resolution of 3 h and at a moderate spatial resolution of ~25 × 25 km^2 for the period between 1998 and 2007. We route discharge with Shuttle Radar Topography Mission (SRTM) topographic data to calculate kilometre-scale specific stream power amounts, a measure of energy expenditure of a river. Combined, this analysis reveals four key results: (i) along the eastern flanks of the Andes and on the Altiplano-Puna Plateau rainfall increases during negative ENSO anomalies by a factor of approximately three compared to normal years, and by a factor of less than approximately two in the west-central parts of the Amazon drainage basin; (ii) not only do the interseasonal rainfall amounts vary strongly, but also the rainfall magnitude-frequency distribution changes – our rainfall time series for each ~25 × 25 km^2 pixel indicate longer duration and more intense rainfall events during negative ENSO years in the southwestern parts of the Amazon drainage basin; (iii) the integrated effects of increased rainfall in the upstream Andean parts of the Amazon catchment magnify discharge in the drainage network downstream and lead to significant flooding events particularly in the southwestern Amazon drainage basin; (iv) an increase in specific stream power by ~25% compared to normal years in the central, and by ~40% in the southwestern Andean foreland emphasizes the importance of negative ENSO years for floodplain formation. Based on these findings we argue that sedimentary fan evolution along the flanks of the orogen and floodplain formation in the foreland are, and have been, strongly controlled by orographic rainfall during negative ENSO events in the elevated parts of the Amazon catchment. Seasonal rainfall variation occurring in the low to medium parts of the Amazon drainage basin play a lesser role in the overall hydrological budget, as amplitude variations are lower. This underscores the significance of the uplift of the Andes not only as the important source region of sediments, but also as an integral part of the Amazon drainage hydrological dynamics. Thus, the combination of high orographic rainfall in the upstream parts of the catchment and its downstream integrated effect on river discharge creates conditions conducive for high-magnitude mass fluxes that have shaped the Amazon drainage basin in the past and will continue to have a first-order control on erosion and deposition in future.

Introduction

Ocean, continental and ice-core records document abrupt climate change on a variety of timescales during the geological past (e.g. Thompson *et al.* 1998; Petit *et al.* 1999; Crowley 2000; Zachos *et al.* 2001; Stott *et al.* 2002). Some of these studies clearly indicate that the climate can shift into an entirely different mode at decadal to centennial timescales, and that the new regime can persist for several decades or centuries (e.g. Thompson *et al.* 1995; Wang *et al.* 2001; Fleitmann *et al.* 2003). However, information about the regional impacts of such changes on surface processes, such as in the El Niño-Southern Oscillation (ENSO) realm, for example, is often lacking or is still largely ambiguous.

At present, the ENSO is the most important coupled ocean-atmosphere phenomenon to cause globally relevant climate variability on various spatiotemporal scales (e.g. Webster & Yang 1992; Timmermann *et al.* 1999; Tudhope *et al.* 2001; Stott *et al.* 2002; Trenberth *et al.* 2007). ENSO in South America has a strong impact on rainfall, discharge, flooding, and erosional mass flux through the Amazon drainage basin into the Atlantic Ocean (e.g. Rao & Hada 1990; Compagnucci & Vargas 1998; Robertson & Mechoso 1998; Garreaud 2000; Viles & Goudie 2003; Marengo 2004; Aalto *et al.* 2006; Haylock *et al.* 2006).

The Amazon River has the largest drainage area and highest discharge on Earth (e.g. Richey *et al.* 1989; Syvitski & Milliman 2007) and understanding the impact of ENSO variability on discharge will aid quantifying erosion and sediment transport in this important region through space and time. Although sediment routing through the Amazon system is pronounced, there is significant transient storage of sediment with Andean provenance in the low-elevation parts of the basin (e.g. Mertes *et al.* 1996; Dunne *et al.* 1998; Aalto *et al.* 2003; Ronchail *et al.* 2005; Safran *et al.* 2005; Barnes & Pelletier 2006).

Understanding modern sediment transport and storage in relation to rainfall and discharge variation is essential for an assessment of the effects of climate variability at present and in the past, particularly with respect to future climate behaviour in a global warming scenario (e.g. Trenberth & Hoar 1997; Kundzewicz *et al.* 2007; Trenberth *et al.* 2007). Furthermore, better knowledge of the complex relationships between climate variability and geomorphic processes may help conceptualize the long-term behaviour of orogenic foreland basins, especially regarding the development of alluvial-fan formation on geological timescales (e.g. Horton & DeCelles 1997; 2001; Leier *et al.* 2005; Uba *et al.* 2007).

The sediment-transport path within the Amazon drainage system from its source (Andes) to sink (Amazon basin or ultimately the Atlantic Ocean) is highly variable. Erosion rates in and sediment transport from the high-elevation Andes are rapid, and transient sediment storage within the narrow mountain valleys is short on geological timescales (e.g. Gaillardet *et al.* 1997; Safran *et al.* 2005, 2006; Barnes & Pelletier 2006; Townsend-Small *et al.* 2008). Similar to other orogens, sediment transport in the steep, high-elevation regions of the orogen is dominated by the effects of relief (e.g. Ahnert 1970; Finnegan *et al.* 2008), climatic gradient (e.g. Pratt *et al.* 2002; Bookhagen *et al.* 2005a, 2005b) or a combination thereof (Bookhagen *et al.* 2006; Gabet *et al.* 2008). However, climatic oscillations at different timescales play a significant role in modulating sediment flux from the eastern slopes of the Andes into the eastern foreland.

Quaternary climate records indicate that moisture transport onto the Altiplano-Puna Plateau in the interior of the orogen, and thus into the high-elevation eastern flanks of the orogen, must have varied significantly (Markgraf & Seltzer 2001; Abbott *et al.* 2003; Seltzer *et al.* 2003). Accordingly, it is expected that in the southwestern part of the Amazon drainage basin and in the northwest Argentine Andes, former phases of strengthened ENSO circulation resulted in increased precipitation that in turn led to increased erosion and deposition cycles in the intermontane basins (e.g. Bookhagen *et al.* 2001; Haselton *et al.* 2002; Trauth *et al.* 2003; Strecker *et al.* 2007). In addition, increases in precipitation are expected to have correlated with episodes of oscillating lake levels and dissolution of the salt-bearing deposits of the internally drained basins of the Altiplano-Puna highlands (Sylvestre *et al.* 1999; Markgraf & Seltzer 2001; Seltzer *et al.* 2003; Placzek *et al.* 2006). Thus, the mass flux originating in the high Andes must have varied in space and time and probably had a pronounced impact on the sediment budget of the Amazon drainage basin.

Once sediment reaches the foreland in an orogenic setting, river gradients, sediment production and transport capacity decrease (Milliman & Meade 1983; Mertes *et al.* 1996; Dunne *et al.* 1998). In addition, the tendency towards transient sediment storage is increased and material transport is closely associated with floodplain formation (e.g. Aalto *et al.* 2003; Bourgoin *et al.* 2007; Dunne *et al.* 1998). Similarly, sediment in the Amazon fluvial system is transferred between river channels and floodplains mainly through aggradation (construction) and erosion (destruction) of the floodplain (e.g. Aalto *et al.* 2003; Dunne *et al.* 1998). The processes eventually leading to floodplain growth include bar formation and sediment accumulation by channelized or diffusive overbank flows. Conversely, floodplain destruction is controlled by channel migration and bank erosion, both highly dominated by the amount of discharge (Bridge 2003).

Large-scale floodplain monitoring in the Amazon has benefitted from innovative remote-sensing work and provides insights into these processes. For example, Hess *et al.* (2003) used L-band synthetic aperture radar (SAR) imagery to map wetland inundation and vegetation extent, both at low- and high-water conditions, to document that wetlands play an important part in accommodating flooding space during high-water conditions. However, few studies have examined sediment exchange on floodplains over large areas using detailed field work and incorporating observations on processes of floodplain construction and destruction (e.g. Aalto *et al.* 2003; Dunne *et al.* 1998). These studies emphasize the key role of flooding magnitude and frequency in floodplain sediment transport in the low-elevation parts of the Andes as well as in other regions of the Earth (Wolman & Miller 1960; Magilligan 1992; Magilligan *et al.* 1998; Aalto *et al.* 2003). Consequently, the rate at which sediment is eroded from an orogen and transferred to and from the floodplains depends not solely on peak discharge, but also on the frequency of heavy rainfall and flooding events.

The parts of the Amazon catchment that receive most moisture per unit area and have the steepest rainfall gradient, correspond to the eastern flanks of the Andes at elevations between 0.7 and 2 km above sea level (Bookhagen & Strecker 2008). Moisture transport into these areas varies most dramatically during ENSO cycles (Fig. 14.1) and identifying the spatial
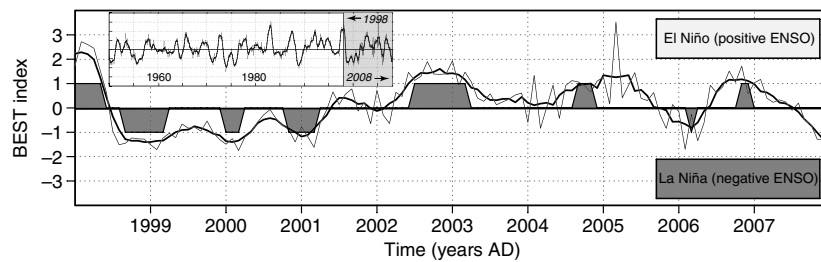
Fig. 14.1   BEST (Bivariate ENSO Timeseries) from 1998 to 2008, the time period covered by the remotely sensed Tropical Rainfall Measurement Mission (TRMM) rainfall data set. Inset indicates BEST index from 1950 to 2008 with the period of 1998–2008 shown in grey (Smith & Sardeshmukh 2000). Negative (positive) BEST index is associated with La Niña (El Niño). Grey bars indicate either negative or positive ENSO anomalies that were used for time-series analysis.

and temporal rainfall characteristics of these sectors is crucial for understanding sediment transport into as well as sediment routing through the Amazon drainage basin. In addition, such knowledge would provide an important insight into the role of climate variability with regards to sediment production in the orogen.

Unfortunately, the spatiotemporal distribution of rainfall in remote areas is difficult to decipher and fraught with many problems. Especially in the Andes and the adjacent Amazon drainage basin, where mountainous terrain and dense vegetation prevent implementation and maintenance of a densely spaced rain-gauge network, measuring rainfall distribution and amount is difficult. Despite the remoteness and difficult infrastructure of the terrain, there are rain-gauge data in some sectors of the Amazon catchment region that provide a coherent view of temporal rainfall variations (e.g. Marengo & Hastenrath 1993; Uvo & Graham 1998; Garreaud & Battisti 1999; Dettinger *et al.* 2000; Grimm *et al.* 2000; Uvo *et al.* 2000; Garreaud & Aceituno 2001; Ronchail *et al.* 2005; Buytaert *et al.* 2006; Haylock *et al.* 2006; Laraque *et al.* 2007). However, in general and particularly within the Andes orogen, the coverage is patchy. This coverage is not sufficient for a detailed rainfall- and discharge-distribution study over a large spatial scale that can be compared to regional erosion studies and sedimentary archives. In recognition of these problems, we attempt to bridge the gap between modern regional rainfall properties, discharge and sediment flux and consider these characteristics with respect to possible past surface processes on geological timescales. First, we investigate modern-day spatiotemporal rainfall characteristics using calibrated, remotely sensed data. Although we only dispose over 10 years of data, this analysis allows deciphering the spatiotemporal rainfall extent during several ENSO cycles as this analysis furnishes information for every 3 hours over every 25 km pixel. Second, we integrate rainfall to derive discharge and use river-channel slopes from topographic data to calculate specific stream power along the longitudinal river profile of the Amazon. Using mean discharge amounts from negative ENSO (La Niña), positive ENSO (El Niño) and normal years, we quantify interseasonal specific stream-power variability. This effort, while using moderately scaled rainfall data, documents the general river-channel response to changing climatic conditions and can be interpreted, with existing field data, in terms of erosional and aggradational processes. Third, we discuss the implications of these findings for geomorphic processes on geological timescales ($>10^5$ years).

Methods

We processed remotely sensed rainfall data from the Tropical Rainfall Measurement Mission (TRMM) 3B42 data product. The TRMM 3B42 data product is widely used and easy to process. It is an algorithm that uses an optimal combination of TRMM 2B31 and TRMM 2A12 data products, SSM/I (Special Sensor Microwave/Imager), AMSR (Advanced Microwave Scanning Radiometer) and AMSU (Advanced Microwave Sounding Unit) rainfall estimates (e.g. Kummerow *et al.* 1998, 2000). The output is gridded rainfall for $0.25 \times 0.25°$ grid boxes (~25×25 km^2) at 3-hour temporal resolution in a global belt extending from 50°S to 50°N. Previously, we have relied on high spatial resolution data collected by the active precipitation radar onboard the TRMM satellite (Bookhagen *et al.* 2006; Bookhagen & Burbank 2006b; Bookhagen & Strecker 2008). While this product has a spatial resolution and grid-cell size of ~5×5 km^2, it produces only 1–3 measurements each day for a given location in the Amazon drainage basin. These data are unique for identifying single rainstorms or topographic–rainfall interactions, but less suitable for time-series analysis.

We have identified the orographic-rainfall barrier and associated elevation along the eastern slopes of the Andes using the high-resolution TRMM 2B31 data (Bookhagen & Strecker 2008). These data were calibrated with 1970 rain-gauge stations throughout South America and the reader is referred to Bookhagen & Strecker (2008) for more information. The TRMM 3B42 data used in this study are already calibrated, and in order to generate absolute rainfall amounts from eight measurements each day (every 3 hours), we linearly interpolated rainfall amounts between measurements and integrated over each day. Although the TRMM 3B42 data set was designed for larger-scale studies and theoretically matches monthly rain-gauge analyses, there are discrepancies in the upper catchment areas. This is expected, as in rough or mountainous terrain, there exists only a weak correlation between point measurements (gauged rainfall) and 3B42 TRMM grid cells (Bookhagen & Strecker 2008).

The rainfall distribution within one 25 km grid cell can vary greatly, especially in regions with a steep topographic gradient. While the 3B42 TRMM depicts the general rainfall gradient, it does not capture accurately the peak rainfall amount and rainfall duration (Chokngamwong & Chiu 2008). However, first-order comparison indicates that the areas we are focusing

on in the Andean foreland with low-relief terrain fit available interpolated rain-gauge data reasonably well (Hoffmann 1975; GDCNV1 2002). The uncertainties associated with the TRMM 3B42 data are disparate in space and time and are difficult to estimate; however, comparable studies in complex terrain show that the TRMM 3B42 compares well with other satellite-derived rainfall products and rain-gauge data (e.g. Dinku *et al.* 2008; Negri *et al.* 2002).

We derived the topographic parameters from a hole-filled 90 m version of the Shuttle Radar Topography Mission (SRTM V3) (Jarvis *et al.* 2006) and resampled the data to 250 m resolution to account for the large catchment size of the Amazon drainage basin (Fig. 14.2). All topographic parameters, such as channel slope, relief and catchment area, were derived from the resampled data set. We have used the ETOPO1 data set (Amante & Eakins

2008) to create a shaded relief topographic and bathymetric map (see Plate 4).

Spatiotemporal rainfall variations in the Andes and the Amazon drainage basin

From a global perspective, there exists a quasi-monsoonal climate in South America (e.g. Rao *et al.* 1996; Zhou & Lau 1998; Grimm *et al.* 2005; Vera *et al.* 2006). In the southern hemisphere summer, an anomalous wind flow originates from the sub-Saharan region and substantially enhances the tropical North Atlantic trades. Thus, the moisture source for rainfall in the Amazon drainage basin and for the eastern flank of the Andes is the Atlantic Ocean (e.g. Grimm *et al.* 2005; Vera *et al.* 2006). The rainy season in the
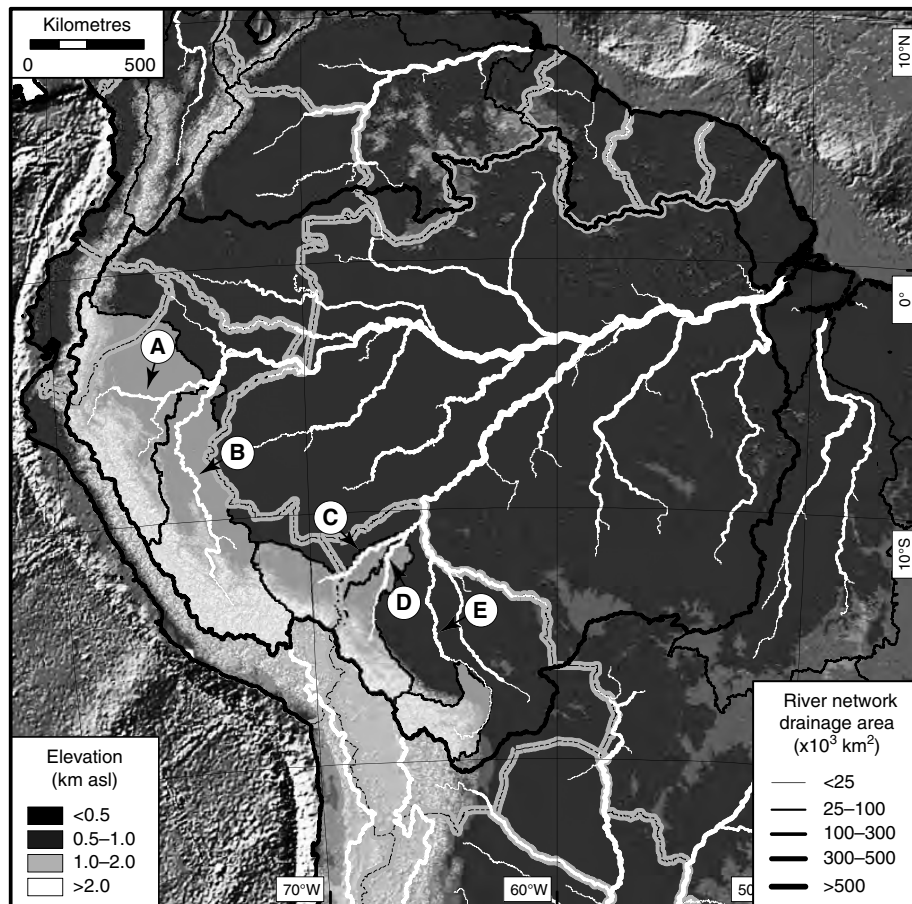

Fig. 14.2   Shaded Shuttle Radar Topography Mission (SRTM) topography of the Amazon drainage system. Drainage basins, as derived from the hydrological analysis of the digital elevation model, are outlined in black; the Amazon drainage basin is outlined in a bold black line. The white line denotes the internally drained Altiplano-Puna Plateau. Grey lines are international borders, white lines mark river networks delineated by drainage areas. Letters indicate tributaries of the Amazon, depicted in more detail in Figs 14.9 & 14.10.

Amazon drainage basin begins in mid-October in the north-west and progresses southeastwards until it reaches the mouth of the Amazon River by the end of December (e.g. Marengo *et al.* 2001). During the austral summer, a warm-core anticyclone, known as the Bolivian High, develops in the upper troposphere over the Altiplano-Puna plateau (e.g. Schwerdfeger 1976; Lenters & Cook 1997; Hardy *et al.* 1998; Garreaud 2000; Grimm *et al.* 2005; Vera *et al.* 2006). Located to the east is an upper-level trough extending over the western South Atlantic from where the mois-ture is drawn. Meanwhile, a continental heat low develops at low levels in the region of the Paraguay-Argentine Gran Chaco (termed the Chaco Low) and northwestern Argentina (termed the Northwestern Argentinean Low) (e.g. Lenters & Cook 1995; Zhou & Lau 1998; Salio *et al.* 2002; Seluchi *et al.* 2003; Marengo *et al.* 2004; Vizy & Cook 2007). In general, the Chaco Low is quasi-permanent during the summer season and associated with heavy annual rainfall amounts (~1.5 m/year), while the Northwestern Argentinean Low is intermittent but exists all year round and has lower rainfall amounts of the order of 0.5 m/year (e.g. Hoffmann 1975; Schwerdtfeger 1976; Lichtenstein 1980; Seluchi *et al.* 2003). The lows exert a dominant control over the South American low-level jet and thus moisture transport into the Andes.

The South American low-level jet first crosses the equator, then becomes a northwesterly flow (flowing to the southeast) along the eastern flank of the Andes, and turns clockwise around the Gran Chaco Low and the Northwestern Argentinean Low, providing moisture as far south as 27°S. The Northwestern Argentinean Low near the Andean slopes is responsible for intensification of the low-level jet and thus moisture transport into the south-central Andes. Moisture transport into the Andean headwaters of the northern, central and southern Amazon drainage basin is directly controlled by the strength of the South American low-level jet (e.g. Garreaud *et al.* 2003; Grimm *et al.* 2005; Marengo *et al.* 2004; Virji 1981; Vizy & Cook 2007). Moisture transport towards and along the Andes varies regionally due to the convex-eastward shape of the Bolivian orocline, which causes high amounts of Andean rainfall north of it (orographic rainfall peak: 4 m/year) and lower amounts (~1 m/year) to the south, although locally higher amounts have been measured (e.g. Marengo 2004; Ronchail & Gallaire 2006; Laraque *et al.* 2007; Bookhagen & Strecker 2008).

At present, the location of the Chaco Low and the Northwestern Argentinean Low is variable in space and time and thus moisture flux into the Andean realm varies (e.g. Seluchi *et al.* 2003; Marengo *et al.* 2004; Cook & Vizy 2006; Vera *et al.* 2006; Vizy & Cook 2007). Based on climate modelling and the existence of multiple moraine generations in the high-elevation, semi-arid highlands of the Eastern Cordillera of Argentina and Bolivia, moisture reaching areas to the north and south of the Andean orocline has been inferred to have greatly varied in the past as well (e.g. Haselton *et al.* 2002; Cook & Vizy 2006; Nicolini & Saulo 2006; Vizy & Cook 2007). This is also supported by lake highstands in the arid Altiplano-Puna Plateau (e.g. Markgraf & Seltzer 2001; Seltzer *et al.* 2003) and adjacent areas (Bookhagen *et al.* 2001; Trauth *et al.* 2003).

The global coupled ocean-atmosphere ENSO phenomenon has a strong impact on environmental and climatic conditions throughout South America (e.g. Rao & Hada 1990; Trenberth 1997; Trenberth & Hoar 1997; Compagnucci & Vargas 1998; Robertson & Mechoso 1998; Garreaud 2000; Vuille *et al.* 2000b;

Grimm 2004; Aalto *et al.* 2006; Haylock *et al.* 2006). It changes sea surface temperature (SST), the position of the Inter-Tropical Convergence Zone (ITCZ), moisture transport and large-scale circulation (e.g. Vuille *et al.* 2000a; Vera *et al.* 2006; Trenberth *et al.* 2007). ENSO is a complex, global-scale phenomenon, which has not been completely understood yet, and we refer the reader to the literature for a more complete description of associated proc-esses, atmospheric patterns and timescales (e.g. Webster & Yang 1992; Trenberth 1997; Trenberth & Hoar 1997; Robertson & Mechoso 1998; Vuille *et al.* 2000b; Coelho *et al.* 2002; Grimm 2003; Vera *et al.* 2006). In our analysis, the impact of ENSO on rainfall (and discharge) is the most important phenomenon and the focus of our investigation. However, we would like to emphasize that other factors such as SST in the Atlantic Ocean strongly control moisture transport into the Amazon drainage basin (e.g. Coelho *et al.* 2002; Grimm *et al.* 2005; Vera *et al.* 2006). For example, in 2005 southwestern Amazonia experienced an intense drought that was not linked to El Niño (as with most previous droughts) but to warming SST in the tropical North Atlantic Ocean (e.g. Cox *et al.* 2008; Marengo *et al.* 2008a, 2008b).

In general, rainfall over east-central Amazonia and northeastern Brazil (southeastern South America and central Chile) tends to be below (above) normal amounts during the warm (cold) phase of ENSO (Trenberth 1997; Coelho *et al.* 2002; Grimm 2003). In order to determine if an ENSO occurred in the past decade, we employed the Bivariate ENSO Timeseries, also referred to as BEST (Smith & Sardeshmukh 2000) (see Fig. 14.1). This data set is based on combining an atmospheric component of the ENSO phenom-enon (the Southern Oscillation Index, or SOI) and an oceanic component (Nino 3.4 SST, which is defined as the SST aver-aged over the region 5°N to 5°S and 170°W to 120°W) (Smith & Sardeshmukh 2000). We have defined the occurrence of a positive or negative ENSO by analysing the period between 1998 and 2007 with a 3-month running mean and using a threshold of the top/bottom 33%. Identification of negative or positive ENSO months does not change if the Multivariate ENSO Index (MEI) is used, which is based on six observed variables over the tropical Pacific (Wolter & Timlin 1998). However, the MEI is less reliable on a month-to-month basis, and we consequently rely on the BEST Index, which combines the two most popular ENSO indices.

Results

For the first time, we have created a consistent rainfall data set for the Amazon drainage basin in South America that relies on calibrated TRMM data. The mean monthly rainfall amount from 10 years of data with approximately 29,200 measurements for each 25×25 km^2 pixel emphasizes the pronounced rainfall gradi-ent between the Amazon drainage basin, the Eastern Cordillera, and the Altiplano-Puna Plateau (Fig. 14.3). In an earlier study, in which we assessed the relation between topography and rainfall distribution along the eastern slopes of the central Andes, we demonstrated that a threshold relief of 1 km within a 3 km radius already constitutes a very effective moisture barrier for easterly and northeasterly moisture-bearing winds (Bookhagen & Strecker 2008). In fact, for more than approximately 2500 km along strike of the eastern Andes, peak rainfall (>4 m/year) occurs in regions
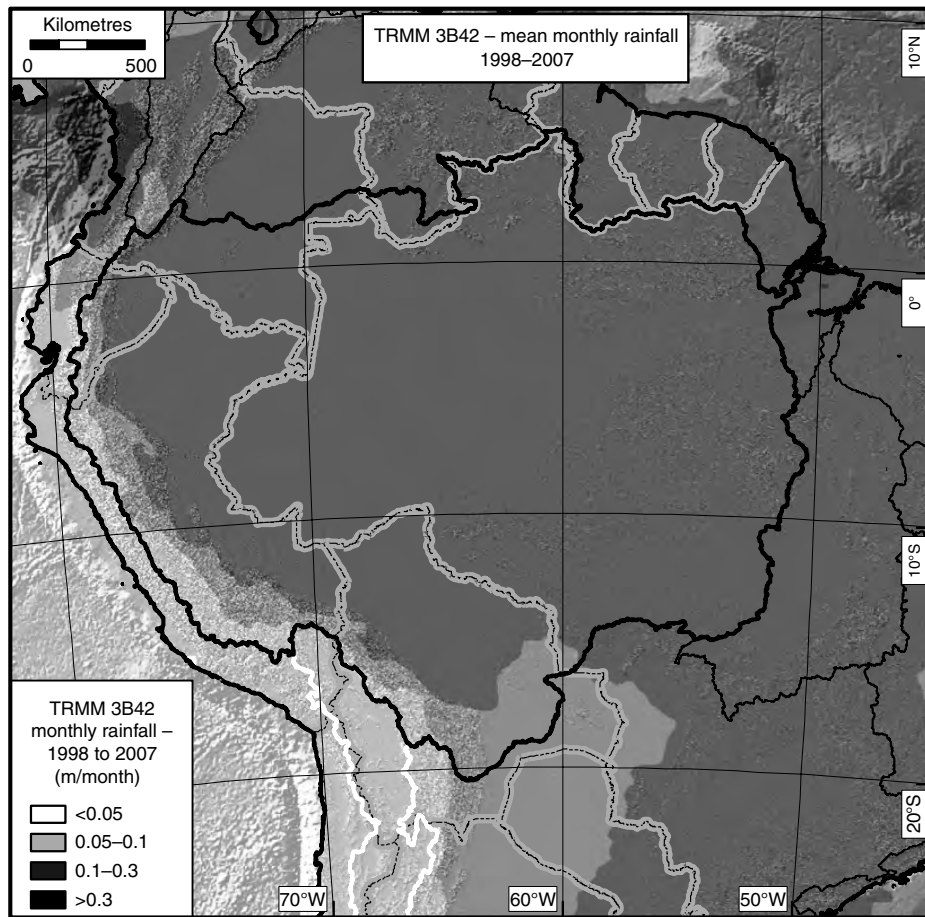
Fig. 14.3 TRMM (Tropical Rainfall Measurement Mission) mean monthly rainfall (m/month) for the period between January 1998 and December 2007. All available TRMM 3B42 data were processed with a high temporal resolution of 3 h and a moderate spatial resolution of ~25 × 25 km² to create this image (~29,000 measurements per pixel). Note the climatic gradient along the eastern flank of the Andes with moderately wet areas near the equator and drier areas in southern subtropical regions.

with more than 1 km of relief. Importantly, areas not exceeding 1 km of relief do not generate a rainfall peak in excess of 2 m/year. Interestingly, this relief threshold is somewhat linked to elevation: peak rainfall occurs at or near 1 km elevation. This finding is supported by rain-gauge analysis in the central Bolivian Andes (Ronchail & Gallaire 2006). Our published record also indicates that the threshold relief at peak rainfall remains nearly constant along the Andes, despite changes in elevation of the peak rainfall location. Thus, topographic relief, combined with elevation, may be a more suitable rainfall proxy than elevation alone, and we refer readers to Bookhagen & Strecker (2008) for a more extensive discussion.

While our previous study was focused on detailed spatial rainfall characteristics, it did not take into account the temporal heterogeneity of rainfall in South America. Spatial rainfall patterns change significantly during negative ENSO (La Niña) years, when higher amounts of moisture reach the western parts of the Amazon

drainage basin and neighbouring areas (Fig. 14.4; see also Plate 5). In order to determine these spatiotemporal rainfall anomalies during ENSO cycles, we compare rainfall amounts during normal (non-ENSO) with negative ENSO years as identified by the BEST index (see Fig. 14.1). We observe that rainfall anomalies during negative ENSO events are strongly correlated with latitude – with northern latitudes receiving lesser amounts and southern latitudes greater amounts than during normal years (Fig. 14.5; see also Plate 5). Importantly, an even stronger rainfall-anomaly gradient exists with respect to altitude. While peak rainfall amounts still occur at the eastern flanks of the orogen, higher-elevation sectors in the Eastern Cordillera and the intraorogenic Altiplano-Puna Plateau locally receive more than twice as much rainfall (see Fig. 14.5 & Plate 5).

During positive ENSO (El Niño) years, rainfall slightly increases throughout the Amazon drainage basin, but less than the rainfall increase associated with a negative ENSO (La Niña) years
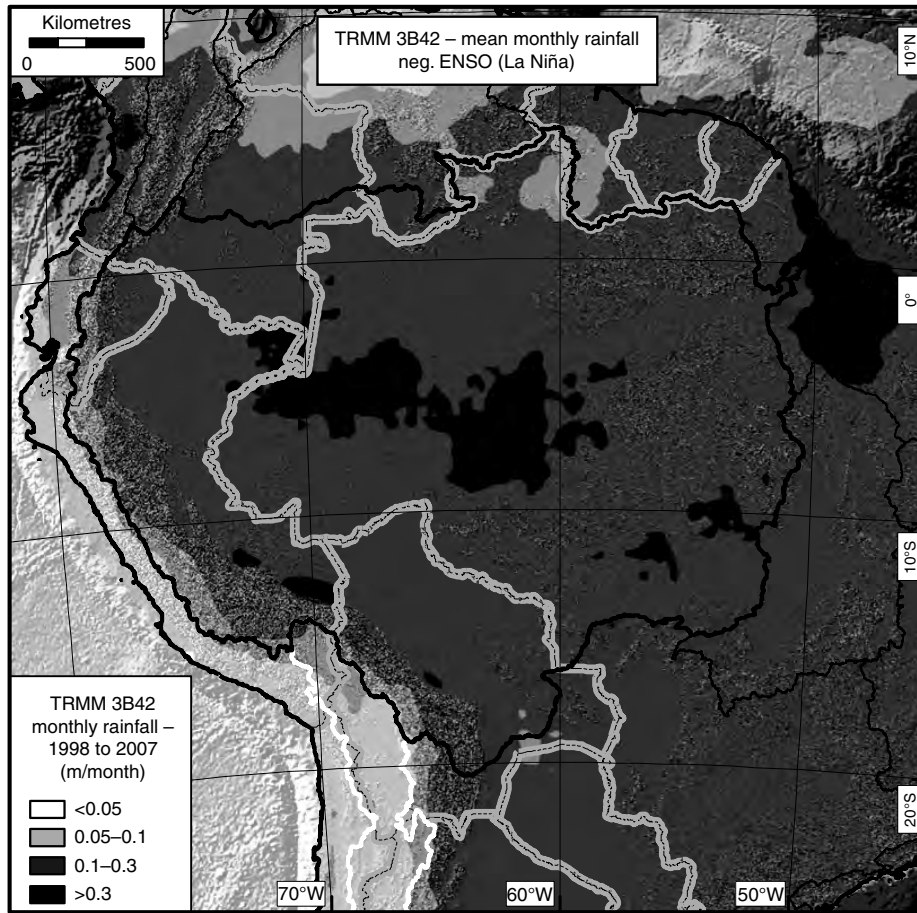
Fig. 14.4   Mean monthly rainfall (m/month) for all negative ENSO (El Niño-Southern Oscillation) anomalies (La Niña) from 1998 as identified by the BEST index (see Fig. 14.1). Note the high rainfall amounts throughout the central and southern Amazon catchment sectors, including the eastern flanks of the Andes in Peru and Bolivia. See also Plate 5.

(Fig. 14.6; see also Plate 5). The most pronounced impact during positive ENSO years is on the western flank of the Andes facing the Pacific, where rainfall increases more than threefold in coastal Ecuador, Colombia and northern Peru (e.g. Hoffmann 1975; Coelho *et al.* 2002; Haylock *et al.* 2006) (Fig. 14.7; see also Plate 5). Although our data integrate only over the past 10 years – the duration of the TRMM mission – parts of our findings are supported by ground-station data. For example, it has been suggested that moisture reaches the Altiplano-Puna Plateau mostly during negative ENSO years (Hardy *et al.* 1998; Garreaud 2000) and that there is a strong rainfall anomaly in the Bolivian Andes (Ronchail & Gallaire 2006). However, these data sets do not provide spatial consistency and are based on a limited number of meteorological stations. While our 10-year data capture only limited negative and positive ENSO cycles, there is internal consistency between each negative or positive ENSO month. Thus, the spatial anomalies documented here are consistent on a month-to-month comparison.

Discussion

We have produced a coherent rainfall–time series that allows us to analyse Amazonian rainfall distribution in space and time. The data only cover 10 years and thus allow us to derive only limited assessments. However, the data coverage permits a detailed and robust analysis that is valid for this time frame. Ultimately, we are interested not only in identifying rainfall-amount variations, but also their magnitude-frequency distribution and impact on discharge in the largest fluvial catchment on Earth. Our rainfall data do not measure erosion and sediment transport, but by combining field observation and measurements made by others (e.g. Aalto *et al.* 2003; Ronchail *et al.* 2005; Townsend-Small *et al.* 2008) with simple model assumptions, we can make first-order predictions on areas of erosion, spatiotemporal variation of sediment transport, and potential long-term impacts of ENSO cycles on the sedimentary and topographic evolution of the Amazon drainage basin. In the following sections we (i) identify the frequency
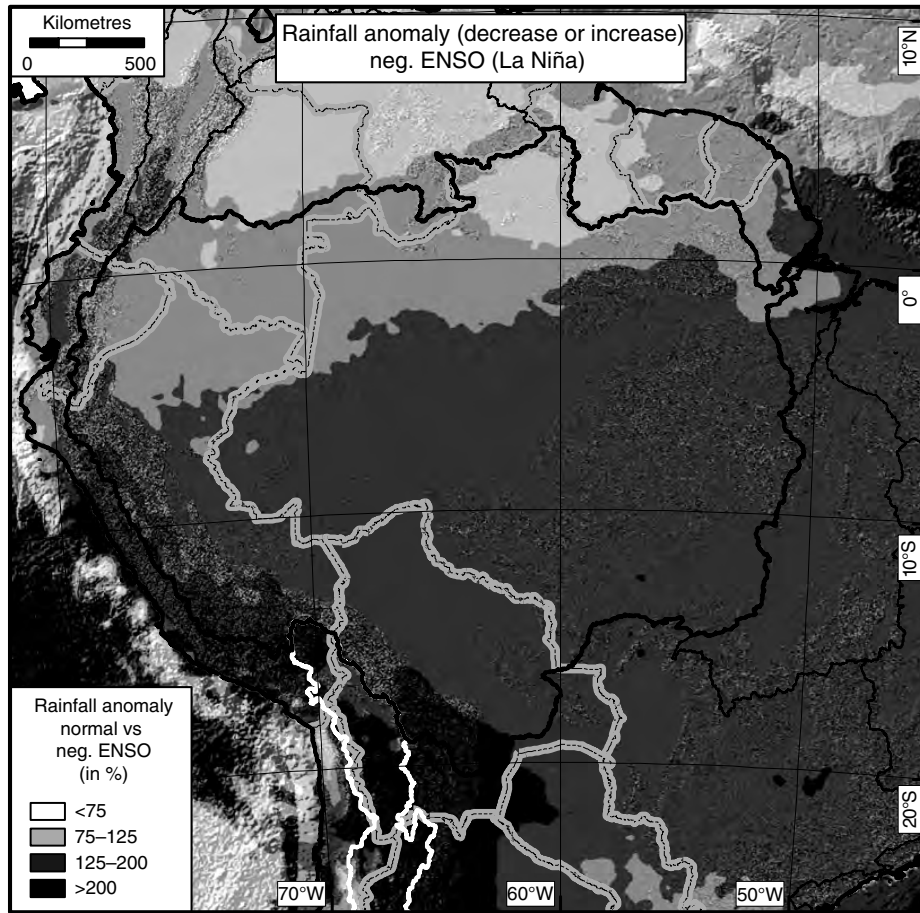
Fig. 14.5 Rainfall anomaly between negative El Niño-Southern Oscillation (ENSO – La Niña) months and non-ENSO months. Rainfall is shown as percentage increase. For example, the grey colours depict rainfall increase by a factor of 1.25 to 2 and dark-grey colours indicate an increase by a factor >2.0. Note the latitudinal zonation and large increase in rainfall during negative ENSO months in the high-elevation sectors of the Andes and along their eastern flanks. See also Plate 5.

of rainfall events; (ii) integrate rainfall to predict river discharge; (iii) calculate specific stream power, a proxy for erosion; and (iv) combine these analyses for a synoptic view of rainfall and surface-process characteristics.

Rainfall frequency

In order to appreciate the relations between erosion and sediment transport, it is important to consider the concept of magnitude-frequency distribution of rainfall events (Wolman & Miller 1960; Magilligan *et al.* 1998; Bull *et al.* 1999; Coppus & Imeson 2002; Aalto *et al.* 2003; Townsend-Small *et al.* 2008). For processes determining landscape evolution it has been argued that erosion dynamics may be dominated by high-magnitude yet low-frequency rainfall events (Wolman & Miller 1960; Coppus & Imeson 2002; Montgomery & Dietrich 2002). For example, in the case of the

southwestern Amazon drainage basin, Aalto *et al.* (2003) suggested that floodplain formation is more directly controlled by rapidly rising rivers during low-frequency, high-magnitude rainfall events rather than by mean discharge amounts. Similarly, field observations and measurements in the Andes of Peru and southern Bolivia indicate that most of the sediment transport occurs during a few heavy rainfall events and that the frequency of these storms is increased during ENSO cycles (e.g. Coppus & Imeson 2002; Espizua & Bengochea 2002; Restrepo *et al.* 2006; Ronchail & Gallaire 2006; Townsend-Small *et al.* 2008).

Our data indicate for the first time the highly disparate distribution of magnitude-frequency events in space and time within the Andean-Amazonian realm. In general, more intense and frequent rainfall during negative ENSO years occurs in the high-elevation Andes and in the southwestern parts of the Amazon drainage basin (Fig. 14.8a). In order to explore the spatial distribution of high-magnitude events, we analysed the time series of each pixel separately
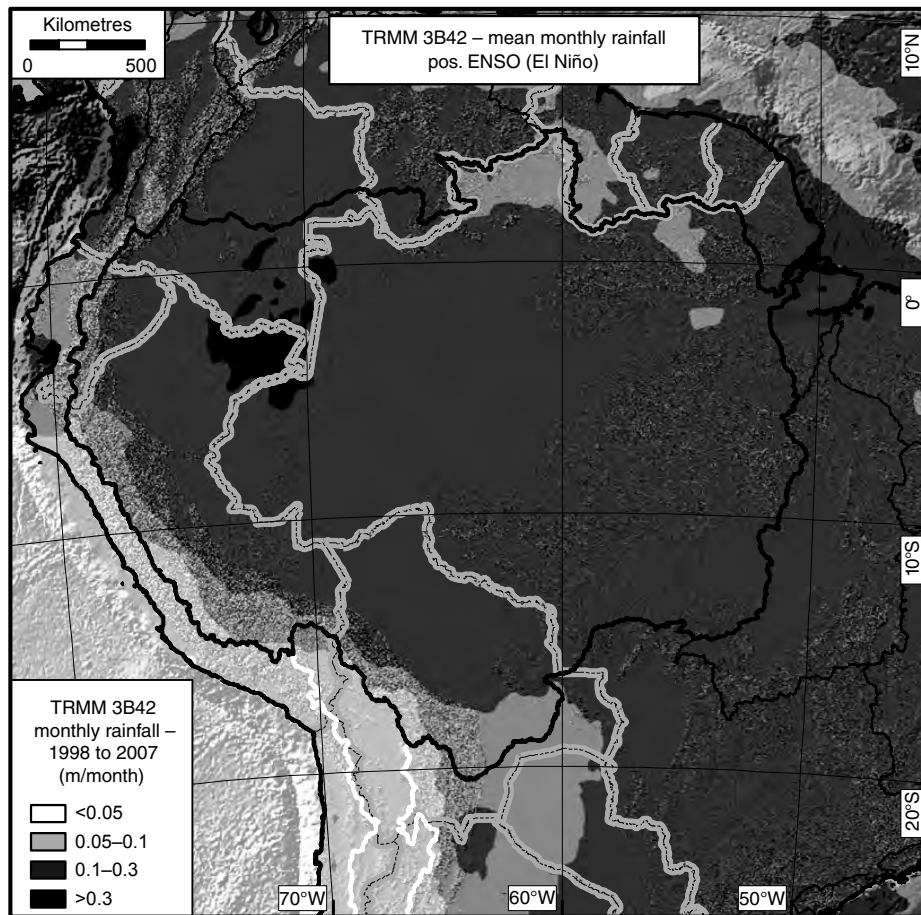
Fig. 14.6   Mean monthly rainfall (m/month) for all positive ENSO (El Niño-Southern Oscillation) anomalies (El Niño) from 1998, as identified by the BEST index. Note the moderate to high rainfall amounts along the Pacific coast of Ecuador and Colombia. In general, the Amazon drainage basin receives lower amounts of rainfall during positive ENSO anomalies, although rainfall is highly disparate in space and time. See also Plate 5.

by first calculating cumulative rainfall amounts, which integrate rainfall over the previous 1-, 2-, 3- or 5-day periods. If a pixel-size area receives high rainfall amounts for several hours or days its value will be high, whereas pixel areas with short-lasting convective rainfall result in lower values. By varying the integration timescale from 1 to 5 days, we take into account the different storm timescales. We observe that the integration over longer time periods (3 or 5 days) limits the relative storm occurrence to the eastern flanks of the Andes and the Altiplano-Puna Plateau, suggesting that longer-lasting storms occur more frequently there. However, the spatial distribution of longer-lasting storms does not change significantly and we thus only rely on the 3-day cumulative rainfall for further analysis. Second, we identified the number of rainfall events above the long-term pixel mean during negative, positive or non-ENSO years (see Fig. 14.8), in order to compare different ENSO cycles. Note that we calculated the mean for each pixel individually from each time series with approximately 29,200 measurements and thus account for varying rainfall amounts

and individual pixel history throughout the Amazon drainage basin. Also, consecutive rainfall amounts above the mean are calculated as a single event.

Clearly, there are significantly more storm events with rainfall amounts above the long-term mean on the eastern flank of the Andes, the southwestern part of the Amazon catchment, and on the Altiplano-Puna Plateau during negative ENSO anomalies (see Fig. 14.8a). Conversely, during positive ENSO years, rainfall frequency and intensity are higher to the west of the Andes in northern coastal Peru (see Fig. 14.8b) (Romero *et al.* 2007). However, rainfall frequency in the Amazon drainage basin did not significantly increase during positive ENSO years. Non-ENSO years show a very homogeneous frequency distribution throughout the entire Amazon catchment (see Fig. 14.8c), indicating lower storm frequency, and thus lower flooding potential.

Interestingly, the areas experiencing more intense and more frequent rainfall events during an ENSO cycle are also characterized
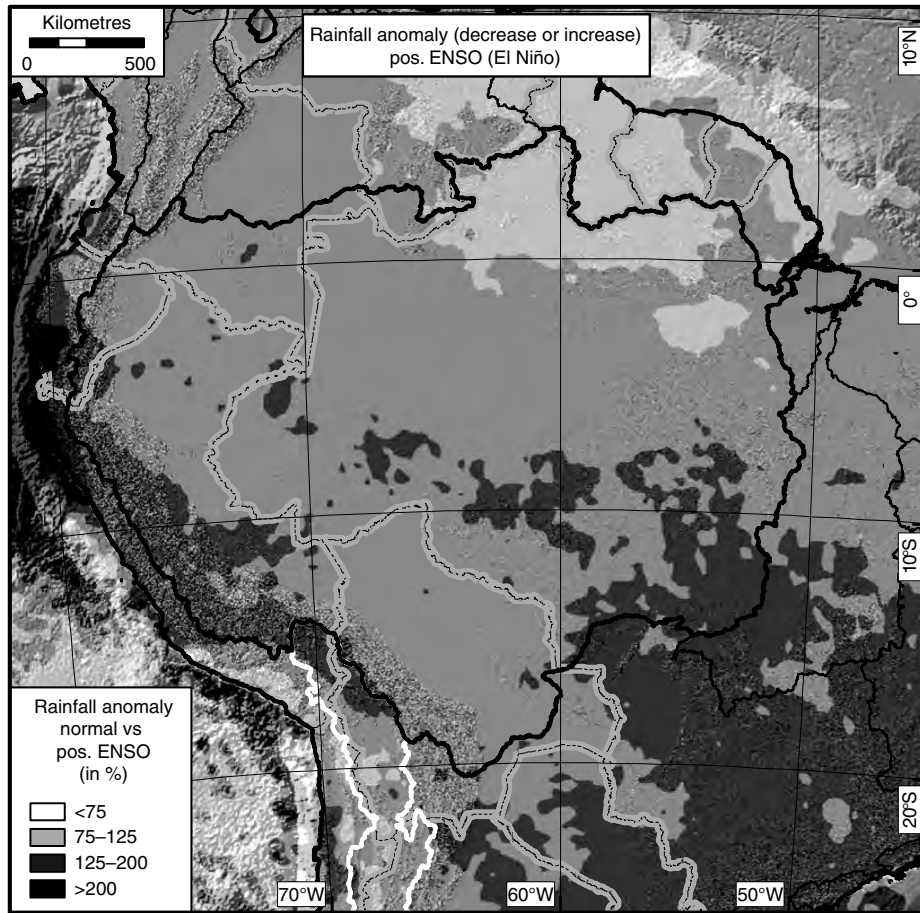
Fig. 14.7 Rainfall anomaly between positive ENSO (El Niño) months and non-ENSO months (also see Fig. 14.5). Rainfall is shown as percentage increase. Rainfall most dominantly increases on the western flanks of the Andes during positive ENSO events. See also Plate 5.

by increased surface-erosion processes (Marwan *et al.* 2003; Viles & Goudie 2003; Moreiras 2005; Houston 2006; Romero *et al.* 2007). Similarly, Aalto *et al.* (2003) have shown that such regions experience more frequent floodplain formation events during negative ENSO years. While erosion rate measurements are sparse, the data sets available clearly indicate that above-normal rainfall events play a significant role in eroding steep mountainous terrain and delivering sediments efficiently to the foreland (Coppus & Imeson 2002; Espizua & Bengochea 2002; Restrepo *et al.* 2006). This observation has important implications for sediment transport to and sediment flux through the Amazon drainage basin on short and long timescales, discussed below.

ENSO and discharge

The spatiotemporal variations of rainfall amounts result in highly varying river discharge, and understanding their relation is difficult as reliable gauge data for smaller or medium-sized catchments

are scarce (Marengo *et al.* 1998; Uvo *et al.* 2000; Marengo 2005). Nevertheless, in order to understand discharge variation in space and time, we integrate our rainfall data and route all run-off to calculate discharge for normal, negative and positive ENSO months. Water routing is dictated by the resampled 250 m SRTM Digital Elevation Model (DEM). This approach will predict exaggerated amounts of discharge for at least two reasons: First, we do not account for evapotranspiration and have calculated discharge simply by summing all upstream run-off. Evapotranspiration amounts can be between 3.1 and 4.7 mm/day on the slow-flowing, low-elevation segments of the Amazon River, although absolute amounts are difficult to determine accurately over large regions (Gat & Matsui 1991; Matsuyama 1992; Costa & Foley 1999). Second, and related to the issue of evaporation, up to 50% of rainfall in the Amazon drainage basin is derived from recycled moisture – our integrated rainfall data thus count these amounts twice or more (Salati & Vose 1984; Eltahir & Bras 1994; Marengo 2005; Bourgoin *et al.* 2007).

While these factors (and most likely several additional ones) prevent us from precisely predicting absolute discharge amounts
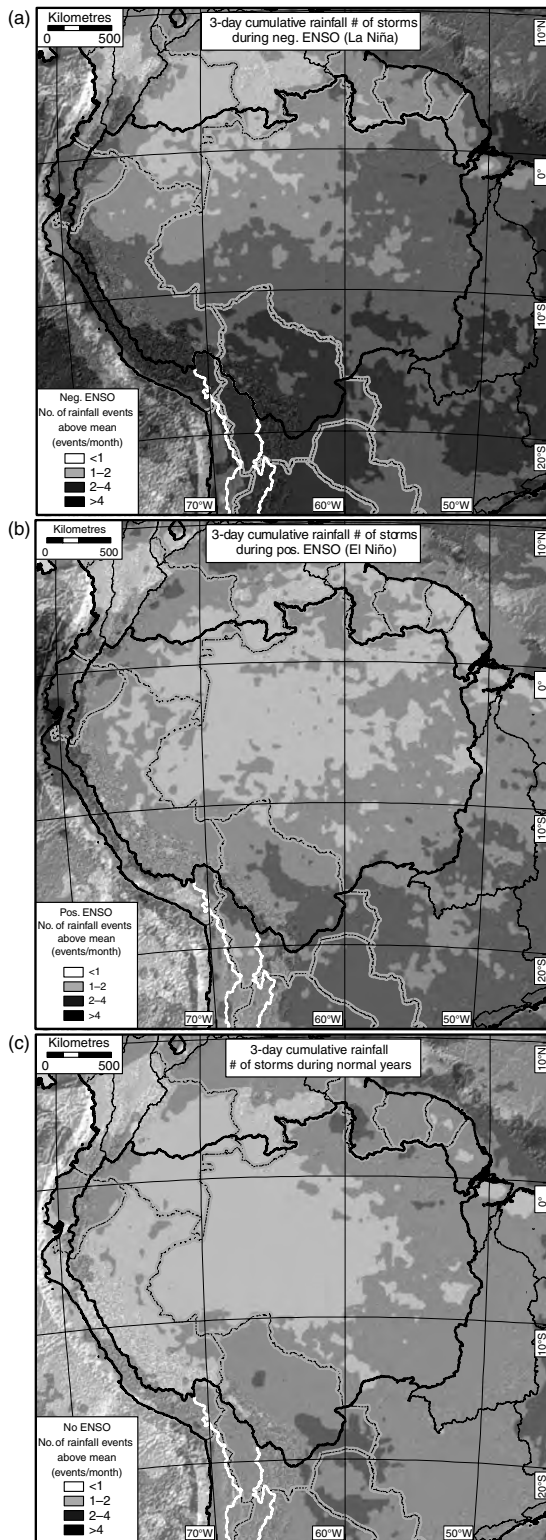
from remotely sensed data, we can compare relative discharge amounts by assuming that the same factors with potentially similar magnitudes affect discharge throughout the years. Thus, we do not apply any correction to the discharge data as evapotranspiration, moisture recycling and other processes are highly disparate in space and time. In general, discharge measured at the mouth of the Amazon River varies between 190 and 200×10^3 m^3/s, while run-off is between 940 and 1040 mm/year (Milliman & Meade 1983; Richey *et al.* 1989; Costa & Foley 1999). Our analysis suggests that discharge amounts for the entire Amazon catchment increase by a relative amount of ~38% during negative and by ~7% during positive ENSO years (Fig. 14.9f). We caution that these general patterns are based on only 10 years of data, but are somewhat supported by longer-term discharge measurements (Richey *et al.* 1989; Marengo 2005). The significant discharge increase during negative ENSO years has been reported earlier with similar magnitudes, based on an 83-year discharge record in the central Amazon drainage basin (Richey *et al.* 1989). While it has been previously argued that discharge decreases during positive ENSO years (Richey *et al.* 1989), our data suggest that the highly heterogeneous rainfall distribution results in different discharge responses of the tributaries. For example, Richey *et al.* (1989) document a strong correlation between low discharge of the Negro River, measured at Manaus in the east-central Amazon drainage basin, with positive ENSO events, which is supported by our remotely sensed rainfall data. Marengo (2005) showed that positive ENSO-related circulation and rainfall anomalies influence the northern Amazon drainage basin, while the southern region seems to be less affected. At interannual timescales, rainfall in the northern basin modulates the water budget in the whole basin as it is generally wetter than the southern parts.

To decipher latitudinal and altitudinal rainfall variations in more detail, we focus on discharge amounts in the five largest tributaries draining extensive sectors of the northern and central Andes. These are, from north to south: (A) Marañón River (size: 360×10^3 km^2), (B) Ucayali River (358×10^3 km^2), (C) Mamoré River (124×10^3 km^2), (D) Beni River (116×10^3 km^2) and (E) Grande River (92×10^3 km^2) catchments (for locations of the rivers, see Fig. 14.2). Our data indicate a strong correlation between increased discharge and negative ENSO years throughout all catchments (see Fig. 14.9). However, discharge

Fig. 14.8 Rainfall-frequency anomaly map for **(a)** negative ENSO, **(b)** positive ENSO and **(c)** non-ENSO (normal) years. Black and dark-grey colours indicate areas that receive higher magnitude and more frequent rainfall events. These maps were generated by calculating the 3-day cumulative rainfall and identifying rainfall events exceeding the long-term mean for each pixel. During negative ENSO conditions, the southwestern Amazon basin and the high-elevation sectors of the Andes have five or more rainstorms that exceed the long-term mean for this pixel. Note the high number of rainstorms on the west coast of the Andes during positive ENSO conditions. In contrast, during non-ENSO (normal) years, rainfall is more homogeneously distributed.
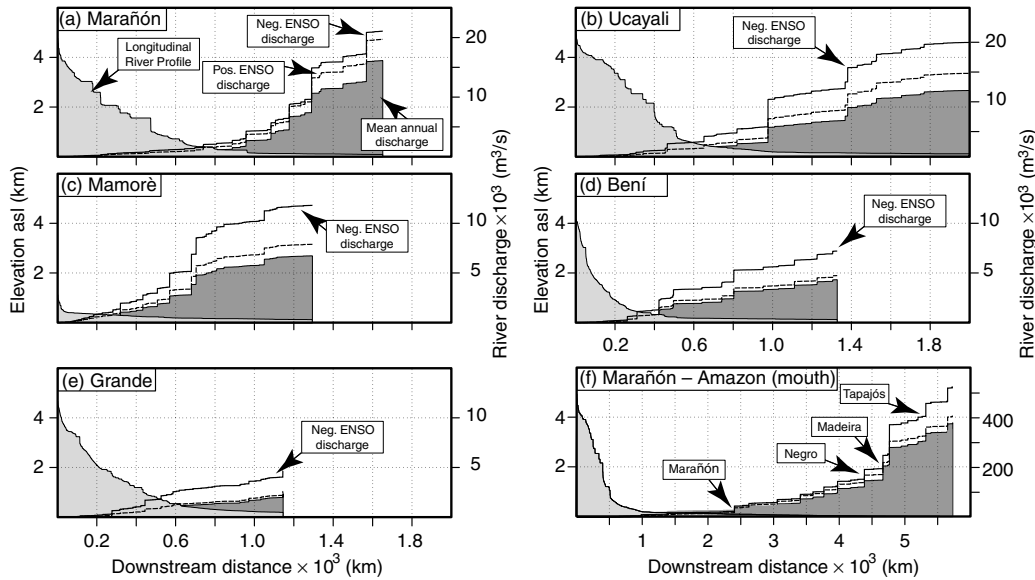
Fig. 14.9 Longitudinal river profiles (LRP) and Tropical Rainfall Measurement Mission (TRMM)-derived discharge for five Amazon tributaries **(a to e)**. River locations are depicted in Fig. 14.2. Filled, dark-shaded polygons indicate river discharge, heavy black line denotes mean monthly discharge during negative ENSO anomalies (La Niña) and dashed lines denote mean monthly discharge during positive ENSO anomalies (El Niño). **(f)** shows the LRP of the entire Amazon basin from the source in south-central Peru (headwaters of the Marañón River) to the mouth at the Atlantic Ocean. Confluences with major rivers are indicated by arrows. Discharge amounts were explicitly routed through the entire catchment using Shuttle Radar Topography Mission (SRTM) data.

in the two southern catchments (Beni River and Grande River) is 1.5 to almost 2 times higher (50 to 100% increase). Discharge increase in the northern catchments is of the order of 30 to 50%. In contrast, the discharge response during positive ENSO anomalies is opposite, as there is a discharge increase in the northern and central Andes tributaries (Marañón and Ucayali rivers), while the southern Andes tributaries (Beni and Grande Rivers) display no significant increase during positive ENSO years (see Fig. 14.9d,e).

The highly disparate discharge response during ENSO cycles results in a complex pattern where northern and southern tributaries of the Amazon River may respond in opposite ways (Richey *et al.* 1989; Robertson & Mechoso 1998). Overall, our remotely sensed data and river-gauge measurements indicate that discharge of the mouth of the Amazon significantly increases during negative ENSO cycles, while the discharge increase is less during positive ENSO years. Again, we emphasize that our data integrate only over 10 years and that a longer time series would provide more robust results.

Figure 14.9f indicates that the most significant increase in discharge of the Marañón-Amazon River system during negative ENSO years occurs at the confluence with the Madeira River 4700 km downstream, when the largest tributary joins the Amazon River. The catchment of the Madeira River displays the highest amounts of rainfall anomalies (see Fig. 14.5 & Plate 5) and experiences the highest numbers of storms (see Fig. 14.8a) during negative ENSO years. Within the Madeira River catchment,

the Beni River and Grande River catchments have the highest numbers of anomalies.

Spatiotemporal variation in specific stream power (SSP)

Discharge is an important factor in determining the hydrological response to rainfall variations in a catchment, but it is no direct measurement of the erosive ability of rivers. In the following attempt to quantify river erosion, we rely on a simple but powerful method to measure a river's energy expenditure on the channel bottom. This approach by no means considers all relevant parameters, but it allows comparison of first-order boundary conditions for fluvial erosion.

Most numerical models of landscape evolution use bedrock incision rules that are related to the physics of bedrock wear through simple scaling arguments, typically by assuming that incision rate is proportional to some measure of flow intensity, such as unit stream power (e.g. Anderson 1994; Howard *et al.* 1994; Bookhagen *et al.* 2006; Bookhagen & Burbank, unpublished data). Stream power per unit channel length (symbolized by Ω and measured in W/m) is defined by:

$$\Omega = \gamma Q s \tag{14.1}$$

where γ is the specific weight of water ($\gamma = \rho_w g = 9810$ N/m³, where ρ_w is the density of water and g is gravitational acceleration),

Q is water discharge (m³/s), and s is the energy slope (m/m), which may be approximated by the slope of the channel bed (e.g. Bagnold 1966, 1977; Knighton 1998). This equation expresses the rate of potential energy expenditure per unit length of channel (or, more simply, the rate of doing work). The corresponding specific stream power (abbreviated as SSP and measured in W/m² or J/m²/year) is given by:

$$\omega = \Omega/w = \tau_0 \nu \qquad (14.2)$$

where w is channel width (m), τ_0 is mean boundary shear stress (N/m²) and ν is mean flow velocity (m/s). This equation defines the rate at which potential energy is supplied to a unit area of the bed. Thus, stream power and potential energy are directly linked.

Whereas discharge is directly derived from the calibrated satellite-rainfall data, we use a scaling law to relate channel width and discharge to capture geomorphic processes over several magnitudes (Leopold & Maddock 1953; Howard *et al.* 1994). The scaling law exploits the dominance of discharge on channel hydraulic geometry and is based on the assumption that the geometric and hydraulic properties of a river channel will adjust in response to increasing discharge. Thus, a regular downstream trend develops in variables such as hydraulic radius, channel width at the water surface, and mean flow velocity (Leopold & Maddock 1953). Here, we are interested in the channel width that forms an integral part of the SSP, where wider channels distribute their stream power over a larger cross-sectional length and consequently result in lower SSP than narrow channels with equal total stream power. The power-law relation between channel width and discharge has the general form of:

$$w = Q^b \qquad (14.3)$$

where b is the scaling factor. Substantial empirical work suggests that discharge-based width scaling relationships are valid for alluvial rivers and that $b \sim 0.5$ (Knighton 1998). This simple approximation does not take into account flooding and crevasse spills, which have been observed and identified for large reaches of the low-elevation Amazon drainage basin (Hess *et al.* 2003; Aalto *et al.* 2003; Dunne *et al.* 1998; Bourgoin *et al.* 2007). However, it allows us to create a first-order approximation of channel-width variation through ENSO cycles.

Our model is thus most appropriate for the upstream reaches of the Amazon drainage basin, where floodplain formation is not the dominant geomorphic channel process. Regarding the entire basin, SSP amounts are highest in the moderate- to high-elevation sectors of the Andes. At elevations of a few hundred metres above sea level of the eastern Andean flanks, rivers merge and their magnified discharge results in high SSP amounts when crossing active structures in the sub-Andean thrust belt. Peak SSP values are of the order of 200 to 400 W/m², while SSPs in the low-elevation Amazon drainage basin are lower by at least an order of magnitude (Fig. 14.10f). Note that peak SSP values in the Andes are less
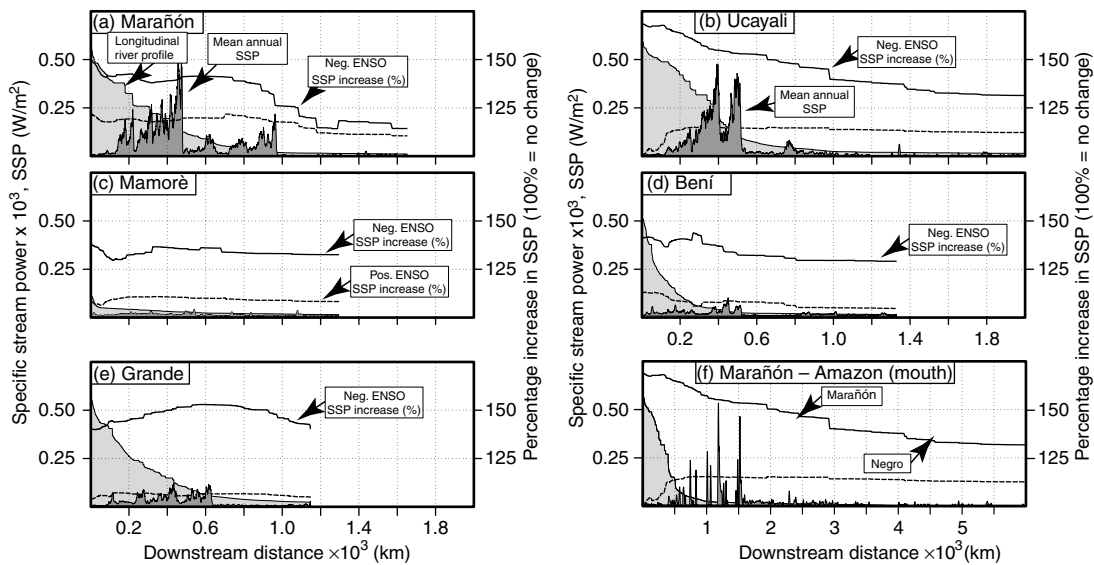

Fig. 14.10 Specific stream power (SSP) for the five major tributaries (**a** to **e**; see Fig. 14.2) and the entire Amazon drainage basin (**f**) during normal, non-ENSO years, in filled dark-grey polygons. SSP is calculated every 10 pixels on the mainstem. Solid lines indicate SSP increase in percent (right *y* axis) during negative ENSO anomalies, and dashed lines the increase during positive ENSO anomalies. Note that rivers generally have a low to moderate response to positive ENSO years, while rainfall during negative ENSO years can increase SSP values by a factor of 1.5 or more in the high-elevation sectors of the Andes. Rainfall in the Río Grande area of the southern Amazon drainage basin causes a significant rise in SSP values. Light-grey polygons show longitudinal river profiles for reference (see Fig. 14.9).

than half the corresponding peak amounts measured throughout the Himalayas, in spite of the fact that river discharges in some Andean catchments are greater (Finnegan *et al.* 2005; Bookhagen *et al.* 2006; Bookhagen & Burbank 2006). Thus, peak SSP values correlate with steep sections of the rivers that are related to tectonically active structures. In addition, the two northern catchments (Marañón and Ucayali Rivers) that we have analysed in more detail have higher SSPs due to their larger size and discharge amounts when exiting the mountain front (see Figs 14.9a,b & 14.10a,b). The southern catchments have lower absolute SSP values (see Fig. 14.10d,e). Varying rainfall distributions during ENSO cycles result in an interesting situation: negative ENSO years correlate with a significant increase in SSP of more than 150% in the medium- to high-elevation areas (see Fig. 14.10). Although in most cases this impact decreases rapidly downstream, the southern Grande River shows a 150% increase over low-elevation areas, where heavy rainfall occurs on the floodplain (see Fig. 14.10e). This region has been documented to be heavily influenced by periodic crevasse spills during negative ENSO years (Aalto *et al.* 2003). In contrast, positive ENSO years do not have a significant impact on SSP variation. Thus, we identify that the medium- to high-elevation eastern flanks of the Andes are more sensitive to erosion rate changes compared to the low-elevation sectors, characterized by low river-channel gradients of the Amazon drainage basin (see Chapter 10).

Landscape evolution through space and time

Although our rainfall data only cover the past decade, they enable critical observations that may be used to understand past surface processes. Using the present-day information about spatiotemporal variations of rainfall, discharge and specific stream power, we provide explanations for erosional and depositional processes that have influenced landscape evolution in the Andean realm.

First, present-day rainfall in the Amazon drainage basin, the Eastern Cordillera of the Andes, and on the Altiplano-Puna Plateau varies significantly. Overall, rainfall follows neither a clear latitudinal nor altitudinal dependence. For example, Fig. 14.8 suggests that even at similar altitudes, rainfall is highly variable, as observed in the region of the Altiplano-Puna Plateau. These present-day disparities in rainfall distribution may well have existed in the past, which makes the assessment of past rainfall scenarios and erosion processes and the interpretation of palaeoclimatic records difficult. It has long been noted that Quaternary palaeoclimatic and geomorphic records of tropical and subtropical South America are often ambiguous with respect to magnitude, timing, spatial extent of wet and dry periods and associated multiple glaciations (Sylvestre *et al.* 1999; Baker *et al.* 2001; Markgraf & Seltzer 2001; Haselton *et al.* 2002; Smith *et al.* 2005).

Second, the geomorphic response to variations in rainfall and discharge provides key components of the evolution of the Amazon drainage basin. The highly disparate spatiotemporal rainfall distribution results in highly variable discharge and sediment flux from the Andes (e.g. Richey *et al.* 1989; Mertes *et al.* 1996; Dunne *et al.* 1998; Syed *et al.* 2005; Restrepo *et al.* 2006; Townsend-Small *et al.* 2008). Especially the Andean sectors of the southwestern Amazon drainage basin and regions in southern Bolivia and NW Argentina dominated by ENSO cycles are affected by these dynamics, including increased storm frequencies and magnitudes. In fact, with the exception of the western Andes and the equatorial Pacific coast, no other region of the Andes displays a more dramatic gradient of rainfall and storm frequency (see Plate 5 & Figs 14.5, 14.7 & 14.8). As the ENSO system has existed at least since the Pliocene (Stott *et al.* 2002; Wara *et al.* 2005), it is expected that associated changes in rainfall, run-off, and geomorphic processes have influenced landscape development in the Andean realm since then. Indeed, this is supported by sedimentary records involving longer timescales ($>10^6$ years), which show that climate has had a pronounced impact on erosion rates in the Amazon drainage basin (Harris & Mix 2002). While tectonism clearly plays an important factor in shaping the Andean orogen, erosion modulated by rainfall distribution (which in turn depends on ENSO patterns) plays a significant role as well. Importantly, during periods with an intensified ENSO circulation those Andean sectors bounding the Amazon drainage basin may be more effectively eroded, resulting in distinct sediment records (Stott *et al.* 2002). Transient storage of sediment on such long timescales is negligible as the average recycling time of modern floodplain deposits in Brazilian Amazonia is <5 ky (Mertes *et al.* 1996).

Generally, while conditions and processes controlling river evolution and dynamics are complex, evidence suggests that large fluctuations in discharge may promote channel instability and avulsion (Mertes *et al.* 1996; Dunne *et al.* 1998; Jones & Schumm 1999; Mohrig *et al.* 2000). Under such conditions, floods related to low-frequency/high-magnitude rainfall events may trigger avulsion (e.g. Magilligan *et al.* 1998; Coppus & Imeson 2002; Aalto *et al.* 2003; Houston 2006; Townsend-Small *et al.* 2008). It is thus conceivable that in the Andean foreland, flooding and discharge variations associated with negative ENSO events may have been an effective catalyst for avulsion as well. In fact, in southern Bolivia and NW Argentina, Miocene to recent foreland-basin sediments are characterized by facies associated with alluvial megafans (Horton & DeCelles 2001; Uba *et al.* 2007). These deposits have been interpreted to result from a seasonal climatic signal associated with the dynamics of the South American monsoon (e.g. Leier *et al.* 2005), but our discharge record indicates that variations between ENSO cycles are much larger than seasonal variations. These variations may trigger avulsion, and over the course of 10^4 to 10^6 years, result in significant aggradation. The distribution of the calculated specific stream power in the southwestern Amazon drainage basin and the eastern flanks of the Altiplano-Puna Plateau shows that SSP values almost double during negative ENSO years. Importantly, the location of the most pronounced SSP increase correlates with the medium- to high-elevation sectors of the eastern flanks of the Andes. Consequently, eroded materials from these sectors are then deposited in the megafans and floodplains (Aalto *et al.* 2003).

A geomorphic-process-based linkage between SSP and landscape erosion rates has not been developed yet, but regions with high SSP, such as the Himalayan orogen, are also characterized by rapid erosion rates (e.g. Thiede *et al.* 2004; Bookhagen *et al.* 2005a, 2005b, 2006; Finnegan *et al.* 2005, 2008; Grujic *et al.* 2006; Blythe *et al.* 2007). Similarly, and important for the

long-term landscape evolution and depositional processes, areas with high erosion rates in the eastern Andes also coincide with regions of high relief and steep channels (e.g. Barnes & Pelletier 2006; Safran *et al.* 2005, 2006). In summary, our present-day observations of rainfall combined with information from landscape evolution, structural data, and sedimentary characteristics provide data for a model that characterizes the long-term behaviour of the fluvial and depositional systems in the Andean foreland areas, which takes the pronounced effects of climate variability into account.

Conclusions

A decade of rainfall data from the Tropical Rainfall Measurement Mission (TRMM) provides an unprecedented view of the inter- and intra-seasonal rainfall variations of the Amazon drainage basin and adjacent areas in the Andes at high spatial and temporal scales. The data show distinct spatiotemporal variation between negative, positive, and normal ENSO states. First, the Altiplano-Puna Plateau and high-elevation sectors in the Eastern Cordillera receive more than twice as much rainfall during negative ENSO (La Niña) anomalies as during non-ENSO years. Similarly, the southwestern parts of the Amazon drainage basin, at lower elevations, receive significantly more rainfall. Positive ENSO (El Niño) anomalies result in significantly increased rainfall in the coastal areas of northern Chile, Peru and Ecuador west of the Andes. The Amazon drainage basin experiences slightly increased rainfall events only in the medium- to high-elevation sectors of the Andean catchment, while the eastern part of the Amazon drainage basin is drier than during normal years. Second, the frequency and intensity of rainfall events during ENSO cycles vary strongly. During negative ENSO years, at least a four-fold increase in heavy storm events occurs in the high-elevation sectors of the Andes, on the Altiplano-Puna Plateau, and in the lowlands of the southwestern part of the Amazon catchment as compared to non-ENSO years. There is a two-fold increase in heavy storm events in the same regions during positive ENSO cycles. During low-frequency, high-magnitude events, mass-transport rates increase. This notion is supported by specific stream power calculations that indicate a doubling during negative ENSO events in the high to moderate elevations of the Andes in the southwestern Amazon catchment, demonstrating that erosion in the Andes and thus sediment flux into the Amazon drainage basin is highly dependent on climate variability. On longer timescales, the recurrence of these processes is interpreted to have caused the formation of megafans along the Andean mountain front south of the drier convex-eastward bend of the orogen, whereas the more humid regions to the north provided sufficient continuous run-off to route sediments into the Amazon drainage basin.

Acknowledgements

References

Aalto, R., Maurice-Bourgoin, L., Dunne, T., Montgomery, D.R., Nittrouer, C.A., Guyot, J.L. (2003) Episodic sediment accumulation on Amazonian flood plains influenced by El Nino/Southern Oscillation. *Nature* 425, 493–497.

Aalto, R., Dunne, T., Guyot, J.L. (2006) Geomorphic controls on Andean denudation rates. *J Geology* 114, 85–99.

Abbott, M.B., Wolfe, B.B., Wolfe, A.P., Seltzer, G.O., Aravena, R., Mark, B.G. *et al.* (2003) Holocene paleohydrology and glacial history of the central Andes using multiproxy lake sediment studies. *Palaeogeogr Palaeocl* 194, 123–138.

Ahnert, F. (1970) Functional relationships between denudation, relief, and uplift in large mid-latitude drainage basins. *Am J Sci* 268, 243–265.

Amante, C., Eakins, B.W. (2008) *ETOPO1 1 Arc-Minute Global Relief Model: Procedures, Data Sources and Analysis.* National Geophysical Data Center, NESDIS, NOAA, Boulder, CO: US Department of Commerce.

Anderson, R.S. (1994) Evolution of the Santa-Cruz Mountains, California, through tectonic growth and geomorphic decay. *J Geophysl Res-Sol Ea* 99, 20161–20179.

Bagnold, R.A. (1966) An approach to the sediment transport problem from general physics. *Geol Surv Prof Paper* 422, 11–137.

Bagnold, R.A. (1977) Bed load transport by natural rivers. *Water Resour Res* 13, 303–312.

Baker, P.A., Seltzer, G.O., Fritz, S.C., Dunbar, R.B., Grove, M.J., Tapia, P.M. *et al.* (2001) The history of South American tropical precipitation for the past 25,000 years. *Science* 291, 640–643.

Barnes, J.B., Pelletier, J.D. (2006) Latitudinal variation of denudation in the evolution of the Bolivian Andes. *Am J Sci* 306, 1–31.

Blythe, A.E., Burbank, D.W., Carter, A., Schmidt, K., Putkonen, J. (2007) Plio-Quaternary exhumation history of the central Nepalese Himalaya: 1. Apatite and zircon fission track and apatite [U-Th]/He analyses. *Tectonics* 26; doi:10.1029/2006TC001990.

Bookhagen, B., Burbank, D.W. (2006) Topography, relief, and TRMM-derived rainfall variations along the Himalaya. *Geophys Res Lett* 33; doi:10.1029/2006GL026037.

Bookhagen, B., Strecker, M.R. (2008) Orographic barriers, high-resolution TRMM rainfall, and relief variations along the eastern Andes. *Geophys Res Lett* 35, L06403, doi:10.1029/2007GL032011.

Bookhagen, B., Haselton, K., Trauth, M.H. (2001) Hydrological modelling of a Pleistocene landslide-dammed lake in the Santa Maria Basin, NW Argentina. *Palaeogeogr Palaeocl* 169, 113–127.

Bookhagen, B., Thiede, R.C., Strecker, M.R. (2005a) Late Quaternary intensified monsoon phases control landscape evolution in the northwest Himalaya. *Geology* 33, 149–152.

Bookhagen, B., Thiede, R.C., Strecker, M.R. (2005b) Abnormal monsoon years and their control on erosion and sediment flux

in the high, and northwest Himalaya. *Earth Planet Sci Lett* 231, 131–146.

Bookhagen, B., Burbank, D., Strecker, M.R., Thiede, R.C., Nishiizumi, K. (2006) Contrasts between short- and long-term erosion rates in the NW Himalaya: disequilibrium at 10^3 to 10^6-yr time scales. *Eos Transactions.* American Geophysical Union, 87(52), Fall Meeting. Suppl., Abstract T13E-03.

Bourgoin, L.M., Bonnet, M.P., Martinez, J.M., Kosuth, P., Cochonneau, G., Moreira-Turcq, P. *et al.* (2007) Temporal dynamics of water and sediment exchanges between the Curuai floodplain and the Amazon River, Brazil. *J Hydrol* 335, 140–156.

Bridge, J.S. (2003) *Rivers and Floodplains.* Oxford: Blackwell.

Bull, L.J., Kirkby, M.J., Shannon, J., Hooke, J.M. (1999) The impact of rainstorms on floods in ephemeral channels in southeast Spain. *Catena* 38, 191–209.

Buytaert, W., Celleri, R., Willems, P., De Bievre, B., Wyseure, G. (2006) Spatial and temporal rainfall variability in mountainous areas: A case study from the south Ecuadorian Andes. *J Hydrol* 329, 413–421.

Chokngamwong, R., Chiu, L.S. (2008) Thailand daily rainfall and comparison with TRMM products. *J Hydrometeorol* 9, 256–266.

Coelho, C.A.S., Uvo, C.B., Ambrizzi, T. (2002) Exploring the impacts of the tropical Pacific SST on the precipitation patterns over South America during ENSO periods. *Theor Appl Climatol* 71, 185–197.

Compagnucci, R.H., Vargas, W.M. (1998) Inter-annual variability of the Cuyo rivers' streamflow in the Argentinean Andean mountains and ENSO events. *Intl J Climatol* 18, 1593–1609.

Cook, K.H., Vizy, E.K. (2006) South American climate during the Last Glacial Maximum: Delayed onset of the South American monsoon. *J Geophys Res-Atmos* 111, D02110, doi:10.1029/2005JD005980.

Coppus, R., Imeson, A.C. (2002) Extreme events controlling erosion and sediment transport in a semi-arid sub-andean valley. *Earth Surf Proc Land* 27, 1365–1375.

Costa, M.H., Foley, J.A. (1999) Trends in the hydrologic cycle of the Amazon basin. *J Geophys Res-Atmos* 104, 189–14,198.

Cox, P.M., Harris, P.P., Huntingford, C., Betts, R.A., Collins, M., Jones, C.D. *et al.* (2008) Increasing risk of Amazonian drought due to decreasing aerosol pollution. *Nature* 453, 212–U217.

Crowley, T.J. (2000) Causes of climate change over the past 1000 years. *Science* 289, 270–277.

Dettinger, M.D., Cayan, D.R., McCabe, G.J. Jr, Marengo, J.A. (2000) Multiscale streamflow variability associated with El Niño/ Southern Oscillation. In: Diaz, H.F., Markgraf, V. (eds) *El Niño and the Southern Oscillation – Multiscale Variability and Global and Regional Impacts.* Cambridge: Cambridge University Press, pp. 113–146.

Dinku, T., Chidzambwa, S., Ceccato, P., Connor, S.J., Ropelewski, C.F. (2008) Validation of high-resolution satellite rainfall products over complex terrain. *Int J Remote Sens* 29, 4097–4110.

Dunne, T., Mertes, L.A.K., Meade, R.H., Richey, J.E., Forsberg, B.R. (1998) Exchanges of sediment between the flood plain and channel of the Amazon River in Brazil. *Geol Soc Am Bull* 110, 450–467.

Eltahir, E.A.B., Bras, R.L. (1994) Precipitation recycling in the Amazon Basin. *Q J Roy Meteor Soc* 120, 861–880.

Espizua, L.E., Bengochea, J.D. (2002) Landslide hazard and risk zonation mapping in the Rio Grande Basin, Central Andes of Mendoza, Argentina. *Mountain Res Dev* 22, 177–185.

Finnegan, N.J., Roe, G., Montgomery, D.R., Hallet, B. (2005) Controls on the channel width of rivers: Implications for modeling fluvial incision of bedrock. *Geology* 33, 229–232.

Finnegan, N.J., Hallet, B., Montgomery, D.R., Zeitler, P.K., Stone, J.O., Anders, A.M., Yuping, L. (2008) Coupling of rock uplift and river incision in the Namche Barwa-Gyala Peri massif, Tibet. *Geol Soc Am Bull* 120, 142–155.

Fleitmann, D., Burns, S.J., Mudelsee, M., Neff, U., Kramers, J., Mangini, A., Matter, A. (2003) Holocene forcing of the Indian monsoon recorded in a stalagmite from Southern Oman. *Science* 300, 1737–1739.

Gabet, E.J., Burbank, D., Pratt-Sitaula, B., Putkonen, J.K., Bookhagen, B. (2008) Modern erosion rates in the High Himalayas of Nepal. *Earth Planet Sci Lett* 267, 482–494.

Gaillardet, J., Dupre, B., Allegre, C.J., Negrel, P. (1997) Chemical and physical denudation in the Amazon River basin. *Chem Geol* 142, 141–173.

Garreaud, R.D. (2000) Intraseasonal variability of moisture and rainfall over the South American Altiplano. *Mon Weather Rev* 128, 3337–3346.

Garreaud, R.D., Aceituno, P. (2001) Interannual rainfall variability over the South American Altiplano. *J Climate* 14, 2779–2789.

Garreaud, R.D., Battisti, D.S. (1999) Interannual (ENSO) and interdecadal (ENSO-like) variability in the Southern Hemisphere tropospheric circulation. *J Climate* 12, 2113–2123.

Garreaud, R., Vuille, M., Clement, A.C. (2003) The climate of the Altiplano: observed current conditions and mechanisms of past changes. *Palaeogeogr Palaeocl* 194, 5–22.

Gat, J.R., Matsui, E. (1991) Atmospheric water balance in the Amazon basin: An isotopic evapotranspiration model. *J Geophys Res-Atmos* 96, 13179–13188.

GDCNV1 (2002) Global Daily Climatology Network (GDCN), V1.0, National Climatic Data Center (released July 2002); URL: http://www.ncdc.noaa.gov/oa/climate/research/gdcn/gdcn.html.

Grimm, A.M. (2003) The El Nino impact on the summer monsoon in Brazil: Regional processes versus remote influences. *J Climate* 16, 263–280.

Grimm, A.M. (2004) How do La Nina events disturb the summer monsoon system in Brazil? *Clim Dynam* 22, 123–138.

Grimm, A.M., Barros, V.R., Doyle, M.E. (2000) Climate variability in southern South America associated with El Nino and La Nina events. *J Climate* 13, 35–58.

Grimm, A.M., Vera, C., Mechoso, C.R. (2005) The South American monsoon system. In: Chang, C.P, Wang, B., Laug. N.C.G (eds) *The Global Monsoon System: Research and Forecast.* World Meteorological Organization Technical Document No. 1266, pp. 219–238.

Grujic, D., Coutand, I., Bookhagen, B., Bonnet, S., Blythe, A., Duncan, C. (2006) Climatic forcing of erosion, landscape, and tectonics in the Bhutan Himalayas. *Geology* 34, 801–804.

Hardy, D.R., Vuille, M., Braun, C., Keimig, F., Bradley, R.S. (1998) Annual and daily meteorological cycles at high altitude on a tropical mountain. *Bull Am Meteorol Soc* 79, 1899–1913.

Harris, S.E., Mix, A.C. (2002) Climate and tectonic influences on continental erosion of tropical South America, 0–13 Ma. *Geology* 30, 447–450.

Haselton, K., Hilley, G., Strecker, M.R. (2002) Average Pleistocene climatic patterns in the southern central Andes: Controls on mountain glaciation and paleoclimate implications. *J Geol* 110, 211–226.

Haylock, M.R., Peterson, T.C., Alves, L.M., Ambrizzi, T., Anunciacao, Y.M.T., Baez, J. *et al.* (2006) Trends in total and extreme South American rainfall in 1960–2000 and links with sea surface temperature. *J Climate* 19, 1490–1512.

Hess, L.L., Melack, J.M., Novo, E., Barbosa, C.C.F., Gastil, M. (2003) Dual-season mapping of wetland inundation and vegetation for the central Amazon basin. *Remote Sens Environ* 87, 404–428.

Hoffmann, J.A.J. (1975) *Atlas climático de América del Sur*. OMM-WMO, UNESCO.

Horton, B.K., DeCelles, P.G. (1997) The modern foreland basin system adjacent to the Central Andes. *Geology* 25, 895–898.

Horton, B.K., DeCelles, P.G. (2001) Modern and ancient fluvial megafans in the foreland basin system of the central Andes, southern Bolivia: implications for drainage network evolution in fold-thrust belts. *Basin Res* 13, 43–63.

Houston, J. (2006) The great Atacama flood of 2001 and its implications for Andean hydrology. *Hydrol Process* 20, 591–610.

Howard, A.D., Dietrich, W.E., Seidl, M.A. (1994) Modeling fluvial erosion on regional to continental scales. *J Geophys Res-Sol Ea* 99, 13971–13986.

Jarvis, A., Reuter, H.I., Nelson, A., Guevara, E. (2006) Hole-filled SRTM for the globe Version 3, edited. Available from the CGIAR-CSI SRTM 90m database; URL: http://srtm.csi.cgiar.org.

Jones, L.J., Schumm, S.A. (1999) Causes of avulsion: an overview. In: Smith, N.D., Rodgers, J. (eds) *Fluvial Sedimentology VI: International Association of Sedimentologists Special Publication*. Oxford: Blackwell Science, pp. 171–178.

Knighton, A.D. (1998) *Fluvial Forms and Processes – A New Perspective*. London: Edward Arnold Ltd.

Kummerow, C., Barnes, W., Kozu, T., Shiue, J., Simpson, J.R. (1998) The Tropical Rainfall Measuring Mission (TRMM) Sensor Package. *J Atmos Ocean Tech* 15, 809–817.

Kummerow, C., Simpson, J., Thiele, O., Barnes, W., Chang, A.T.C., Stocker, E. *et al.* (2000) The status of the Tropical Rainfall Measuring Mission (TRMM) after two years in orbit. *J Appl Meteorol* 39, 1965–1982.

Kundzewicz, Z.W., Mata, L.J., Arnell, N.W., Döll, P., Kabat, P., Jiménez, B. *et al.* (2007) Freshwater resources and their management. In: Parry, M.L., Canziani, O.F., Palutikof, J.P., van der Linden, P.J., Hanson, C.E. (eds) *Climate Change 2007: Impacts, Adaptation and Vulnerability. Contribution of Working Group II to the Fourth Assessment Report of the Intergovernmental Panel on Climate Change*. Cambridge: Cambridge University Press, pp. 173–210.

Laraque, A., Ronchail, J., Cochonneau, G., Pombosa, R., Guyot, J.L. (2007) Heterogeneous distribution of rainfall and discharge regimes in the Ecuadorian Amazon basin. *J Hydrometeorol* 8, 1364–1381.

Leier, A.L., DeCelles, P.G., Pelletier, J.D. (2005) Mountains, monsoons, and megafans. *Geology* 33, 289–292.

Lenters, J.D., Cook, K.H. (1995) Simulation and diagnosis of the regional summertime precipitation climatology of South America. *J Climate* 8, 2988–3005.

Lenters, J.D., Cook, K.H. (1997) On the origin of the Bolivian high and related circulation features of the South American climate. *J Atmos Sci* 54, 656–677.

Leopold, L.B., Maddock, T. (1953) The hydraulic geometry of stream channels and some physiographic implications. *US Geol Surv Prof Paper* 252.

Lichtenstein, E.R. (1980) La Depresion del Noroeste Argentina (The Northwestern Argentina Low). PhD thesis, University of Buenos Aires, 223 pp.

Magilligan, F.J. (1992) Thresholds and the spatial variability of flood power during extreme floods. *Geomorphology* 5, 373–390.

Magilligan, F.J., Phillips, J.D., James, L.A., Gomez, B. (1998) Geomorphic and sedimentological controls on the effectiveness of an extreme flood. *J Geol* 106, 87–95.

Marengo, J.A. (2004) Interdecadal variability and trends of rainfall across the Amazon basin. *Theor Appl Climatol* 78, 79–96.

Marengo, J.A. (2005) Characteristics and spatio-temporal variability of the Amazon River Basin water budget. *Clim Dynam* 24, 11–22.

Marengo, J.A., Hastenrath, S. (1993) Case-studies of extreme climatic events in the Amazon Basin. *J Climate* 6, 617–627.

Marengo, J.A., Tomasella, J., Uvo, C.R. (1998) Trends in streamflow and rainfall in tropical South America: Amazonia, eastern Brazil, and northwestern Peru. *J Geophys Res-Atmos* 103, 1775–1783.

Marengo, J.A., Liebmann, B., Kousky, V.E., Filizola, N.P., Wainer, I.C. (2001) Onset and end of the rainy season in the Brazilian Amazon Basin. *J Climate* 14, 833–852.

Marengo, J.A., Soares, W.R., Saulo, C., Nicolini, M. (2004) Climatology of the low-level jet east of the Andes as derived from the NCEP-NCAR reanalyses: Characteristics and temporal variability. *J Climate* 17, 2261–2280.

Marengo, J.A., Nobre, C.A., Tomasella, J., Cardoso, M.F., Oyama, M.D. (2008a) Hydro-climatic and ecological behaviour of the drought of Amazonia in 2005. *Philos T Roy Soc B* 363, 1773–1778.

Marengo, J.A., Nobre, C.A., Tomasella, J., Oyama, M.D., de Oliviera, G.S., de Oliviera, R. *et al.* (2008b) The drought of Amazonia in 2005. *J Climate* 21, 495–516.

Markgraf, V., Seltzer, G.O. (2001) Pole-equator-pole paleoclimates of the Americas integration: toward the big picture. In: Markgraf, V. (ed.) *Interhemispheric Climate Linkages*. San Diego: Academic Press, pp. 433–442.

Marwan, N., Trauth, M.H., Vuille, M., Kurths, J. (2003) Comparing modern and Pleistocene ENSO-like influences in NW Argentina using nonlinear time series analysis methods. *Clim Dynam* 21, 317–326.

Matsuyama, H. (1992) The water budget in the Amazon River basin during the FGGE period. *J Meteorol Soc Jpn* 70, 1071–1083.

Mertes, L.A.K., Dunne, T., Martinelli, L.A. (1996) Channel-floodplain geomorphology along the Solimoes-Amazon River, Brazil. *Geol Soc Am Bull* 108, 1089–1107.

Milliman, J.D., Meade, R.H. (1983) Worldwide delivery of river sediments to the ocean. *J Geol* 91, 1–21.

Mohrig, D., Heller, P.L., Paola, C., Lyons, W.J. (2000) Interpreting avulsion process from ancient alluvial sequences: Guadalope-Matarranya system (northern Spain) and Wasatch Formation (western Colorado). *Geol Soc Am Bull* 112, 1787–1803.

Montgomery, D.R., Dietrich, W.E. (2002) Runoff generation in a steep, soil-mantled landscape. *Water Resour Res* 38, 1168, doi:10.1029/2001WR000822.

Moreiras, S.M. (2005) Climatic effect of ENSO associated with landslide occurrence in the Central Andes, Mendoza Province, Argentina. *Landslides* 2, 53–59.

Negri, A.J., Bell, T.L., Xu, L.M. (2002) Sampling of the diurnal cycle of precipitation using TRMM. *J Atmos Ocean Tech* 19, 1333–1344.

Nicolini, M., Saulo, A.C. (2006) Modeled Chaco low-level jets and related precipitation patterns during the 1997–1998 warm season. *Meteorol Atmos Phys* 94, 129–143.

Petit, J.R., Jouzel, J., Raynaud, D., Barkov, N.I., Barnola, J.M., Basile, I. *et al.* (1999) Climate and atmospheric history of the past 420,000 years from the Vostok ice core, Antarctica. *Nature* 399, 429–436.

Placzek, C., Quade, J., Patchett, P.J. (2006) Geochronology and stratigraphy of late Pleistocene lake cycles on the southern Bolivian Altiplano: Implications for causes of tropical climate change. *Geol Soc Am Bull* 118, 515–532.

Pratt, B., Burbank, D.W., Heimsath, A., Ojha, T. (2002) Impulsive alluviation during early Holocene strengthened monsoons, central Nepal Himalaya. *Geology* 30, 911–914.

Rao, V.B., Hada, K. (1990) Characteristics of rainfall over Brazil – annual variations and connections with the Southern Oscillation. *Theor Appl Climatol* 42, 81–91.

Rao, V.B., Cavalcanti, I.F.A., Hada, K. (1996) Annual variation of rainfall over Brazil and water vapor characteristics over South America. *J Geophys Res-Atmos* 101, 26539–26551.

Restrepo, J.D., Kjerfve, B., Hermelin, M., Restrepo, J.C. (2006) Factors controlling sediment yield in a major South American drainage basin: the Magdalena River, Colombia. *J Hydrol* 316, 213–232.

Richey, J.E., Nobre, C., Deser, C. (1989) Amazon River discharge and climate variability – 1903 to 1985. *Science* 246, 101–103.

Robertson, A.W., Mechoso, C.R. (1998) Interannual and decadal cycles in river flows of southeastern South America. *J Climate* 11, 2570–2581.

Romero, C.C., Baigorria, G.A., Stroosnijder, L. (2007) Changes of erosive rainfall for El Nino and La Nina years in the northern Andean highlands of Peru. *Climatic Change* 85, 343–356.

Ronchail, J., Gallaire, R. (2006) Enso and rainfall along the Zongo valley (Bolivia) from the Altiplano to the Amazon basin. *Int J Climatol* 26, 1223–1236.

Ronchail, J., Bourrel, L., Cochonneau, G., Vauchel, P., Phillips, L., Castro, A. *et al.* (2005) Inundations in the Mamore basin (southwestern Amazon-Bolivia) and sea-surface temperature in the Pacific and Atlantic Oceans. *J Hydrol* 302, 223–238.

Safran, E.B., Bierman, P.R., Aalto, R., Dunne, T., Whipple, K.X., Caffee, M. (2005) Erosion rates driven by channel network incision in the Bolivian Andes. *Earth Surf Process Land* 30, 1007–1024.

Safran, E.B., Blythe, A., Dunne, T. (2006) Spatially variable exhumation rates in orogenic belts: An Andean example. *J Geol* 114, 665–681.

Salati, E., Vose, P.B. (1984) Amazon Basin: a system in equilibrium. *Science* 225, 129–138.

Salio, P., Nicolini, M., Saulo, A.C. (2002) Chaco low-level jet events characterization during the austral summer season. *J Geophys Res-Atmos* 107, 4816, doi:10.1029/2001JD001315.

Schwerdtfeger, W. (1976) *Climates of Central and South America.* Amsterdam: Elsevier Scientific Publishing, 532 pp.

Seltzer, G.O., Rodbell, D.T., Wright, H.E.J. (2003) Late-quaternary paleoclimates of the southern tropical Andes and adjacent regions. *Palaeogeogr Palaeocl* 194, 1–3.

Seluchi, M.E., Saulo, A.C., Nicolini, M., Satyamurty, P. (2003) The northwestern Argentinean low: A study of two typical events. *Mon Weather Rev* 131, 2361–2378.

Smith, C.A., Sardeshmukh, P. (2000) The effect of ENSO on the intraseasonal variance of surface temperature in winter. *Int J Climatol* 20, 1543–1557.

Smith, J.A., Seltzer, G.O., Rodbell, D.T., Klein, A.G. (2005) Regional synthesis of last glacial maximum snowlines in the tropical Andes, South America. *Quaternary Int* 138, 145–167.

Stott, L., Poulsen, C., Lund, S., Thunell, R. (2002) Super ENSO and global climate oscillations at millennial time scales. *Science* 297, 222–226.

Strecker, M.R., Alonso, R.N., Bookhagen, B., Carrapa, B., Hilley, G.E., Sobel, E.R., Trauth, M.H. (2007) Tectonics and climate of the southern central Andes. *Annu Rev Earth Planetary Sci* 35, 747–787.

Syed, T.H., Famiglietti, J.S., Chen, J., Rodell, M., Seneviratne, S. I., Viterbo, P., Wilson, C.R. (2005) Total basin discharge for the Amazon and Mississippi River basins from GRACE and a land-atmosphere water balance. *Geophys Res Lett* 32. doi:10.1029/2005GL024851.

Sylvestre, F., Servant, M., Servant-Vildary, S., Causse, C., Fournier, M., Ybert, J.-P. (1999) Lake-level chronology on the Southern Bolivian Altiplano (18°–23°S) during late-glacial time and the Early Holocene. *Quaternary Res* 51, 54–66.

Syvitski, J.P.M., Milliman, J.D. (2007) Geology, geography, and humans battle for dominance over the delivery of fluvial sediment to the coastal ocean. *J Geol* 115, 1–19.

Thiede, R.C., Bookhagen, B., Arrowsmith, J.R., Sobel, E.R., Strecker, M.R. (2004) Climatic control on rapid exhumation along the Southern Himalayan Front. *Earth Planet Sci Lett* 222, 791–806.

Thompson, L.G., Mosleythompson, E., Davis, M.E., Lin, P.N., Henderson, K.A., Coledai, J. *et al.* (1995) Late-Glacial stage and Holocene tropical ice core records from Huascaran, Peru. *Science* 269, 46–50.

Thompson, L.G., Davis, M.E., Mosley-Thompson, E., Sowers, T.A., Henderson, K.A., Zagorodnov, V.S. *et al.* (1998) A 25,000-year tropical climate history from Bolivian ice cores. *Science* 282, 1858–1864.

Timmermann, A., Oberhuber, J., Bacher, A., Esch, M., Latif, M., Roeckner, E. (1999) Increased El Nino frequency in a climate model forced by future greenhouse warming. *Nature* 398, 694–697.

Townsend-Small, A., McClain, M.E., Hall, B., Noguera, J.L., Llerena, C.A., Brandes, J.A. (2008) Suspended sediments and organic matter in mountain headwaters of the Amazon River: Results from a 1-year time series study in the central Peruvian Andes. *Geochim Cosmochim Ac* 72, 732–740.

Trauth, M.H., Bookhagen, B., Marwan, N., Strecker, M.R. (2003) Multiple landslide clusters record Quaternary climate changes in the northwestern Argentine Andes. *Palaeogeogr Palaeocl* 194, 109–121.

Trenberth, K.E. (1997) The definition of El Nino. *Bull Am Meteorol Soc* 78, 2771–2777.

Trenberth, K.E., Hoar, T.J. (1997) El Nino and climate change. *Geophys Res Lett* 24, 3057–3060.

Trenberth, K.E., Jones, P.D., Ambenje, P., Bojariu, R., Easterling, D., Klein Tank, A. *et al.* (2007) Observations: surface and atmospheric climate change. In: Solomon, S., Qin, D., Manning, M., Chen, Z., Marquis, M., Averyt, K.B. *et al.* (eds) *Climate Change 2007: The Physical Science Basis. Contribution of Working Group I to the Fourth Assessment Report of the Intergovernmental Panel on Climate Change.* Cambridge: Cambridge University Press.

Tudhope, A.W., Chilcott, C.P., McCulloch, M.T., Cook, E.R., Chappell, J., Ellam, R.M. *et al.* (2001) Variability in the El Nino-Southern oscillation through a glacial-interglacial cycle. *Science* 291, 1511–1517.

Uba, C.E., Strecker, M.R., Schmitt, A.K. (2007) Increased sediment accumulation rates and climatic forcing in the central Andes during the late Miocene. *Geology* 35, 979–982.

Uvo, C.B., Graham, N.E. (1998) Seasonal runoff forecast for northern South America: A statistical model. *Water Resour Res* 34, 3515–3524.

Uvo, C.B., Tölle, U., Berndtsson, R. (2000) Forecasting discharge in Amazonia using artificial neural networks. *Int J Climatol* 20, 1495–1507.

Vera, C., Higgins, W., Amador, J., Ambrizzi, T., Garreaud, R., Gochis, D. *et al.* (2006) Toward a unified view of the American Monsoon Systems. *J Climate* 19, 4977–5000.

Viles, H.A., Goudie, A.S. (2003) Interannual, decadal and multidecadal scale climatic variability and geomorphology. *Earth Sci Rev* 61, 105–131.

Virji, H. (1981) A preliminary study of summertime tropospheric circulation patterns over South America estimated from cloud winds. *Mon Weather Rev* 109, 599–610.

Vizy, E.K., Cook, K.H. (2007) Relationship between Amazon and high Andes rainfall. *J Geophys Res-Atmos* 112, D07107, doi:10.1029/2006JD007980.

Vuille, M., Bradley, R.S., Keimig, F. (2000a) Interannual climate variability in the Central Andes and its relation to tropical Pacific and Atlantic forcing. *J Geophys Res-Atmos* 105, 12447–12460.

Vuille, M., Bradley, R.S., Keimig, F. (2000b) Climate variability in the Andes of Ecuador and its relation to tropical Pacific and Atlantic sea surface temperature anomalies. *J Climate* 13, 2520–2535.

Wang, Y.J., Cheng, H., Edwards, R.L., An, Z.S., Wu, J.Y., Shen, C.C., Dorale, J.A. (2001) A high-resolution absolute-dated Late Pleistocene monsoon record from Hulu Cave, China. *Science* 294, 2345–2348.

Wara, M.W., Ravelo, A.C., Delaney, M.L. (2005) Permanent El Nino-like conditions during the Pliocene warm period. *Science* 309, 758–761.

Webster, P.J., Yang, S. (1992) Monsoon and Enso – selectively interactive systems. *Q J Roy Meteor Soc* 118, 877–926.

Wolman, M.G., Miller, J.P. (1960) Magnitude and frequency of forces in geomorphic processes. *J Geol* 68, 54–74.

Wolter, K., Timlin, M.S. (1998) Measuring the strength of ENSO events – how does 1997/98 rank? *Weather* 53, 315–324.

Zachos, J., Pagani, M., Sloan, L., Thomas, E., Billups, K. (2001) Trends, rhythms, and aberrations in global climate 65 Ma to present. *Science* 292, 686–693.

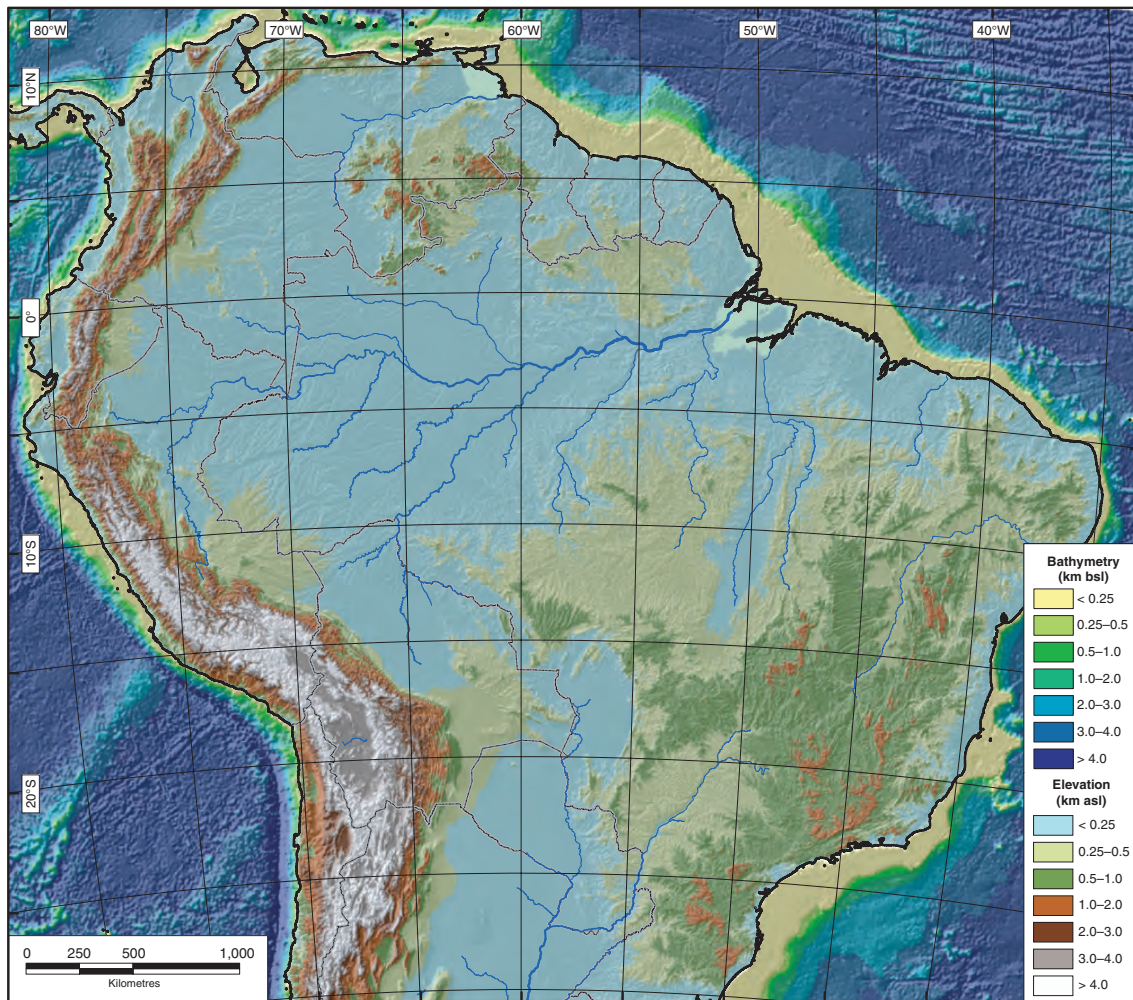Zhou, J.Y., Lau, K.M. (1998) Does a monsoon climate exist over South America? *J Climate* 11, 1020–1040.

Plate 4 Shaded-relief topography and bathymetry of South America produced from ETOPO1 (Amante & Eakins 2008, ETOPO1 1 Arc-Minute Global Relief Model: Procedures, Data Sources and Analysis, National Geophysical Data Center, NESDIS, NOAA, US Department of Commerce, Boulder, CO, August 2008). Grey lines indicate national boundaries, blue lines depict rivers, with their line width proportional to drainage area. Map created by B. Bookhagen
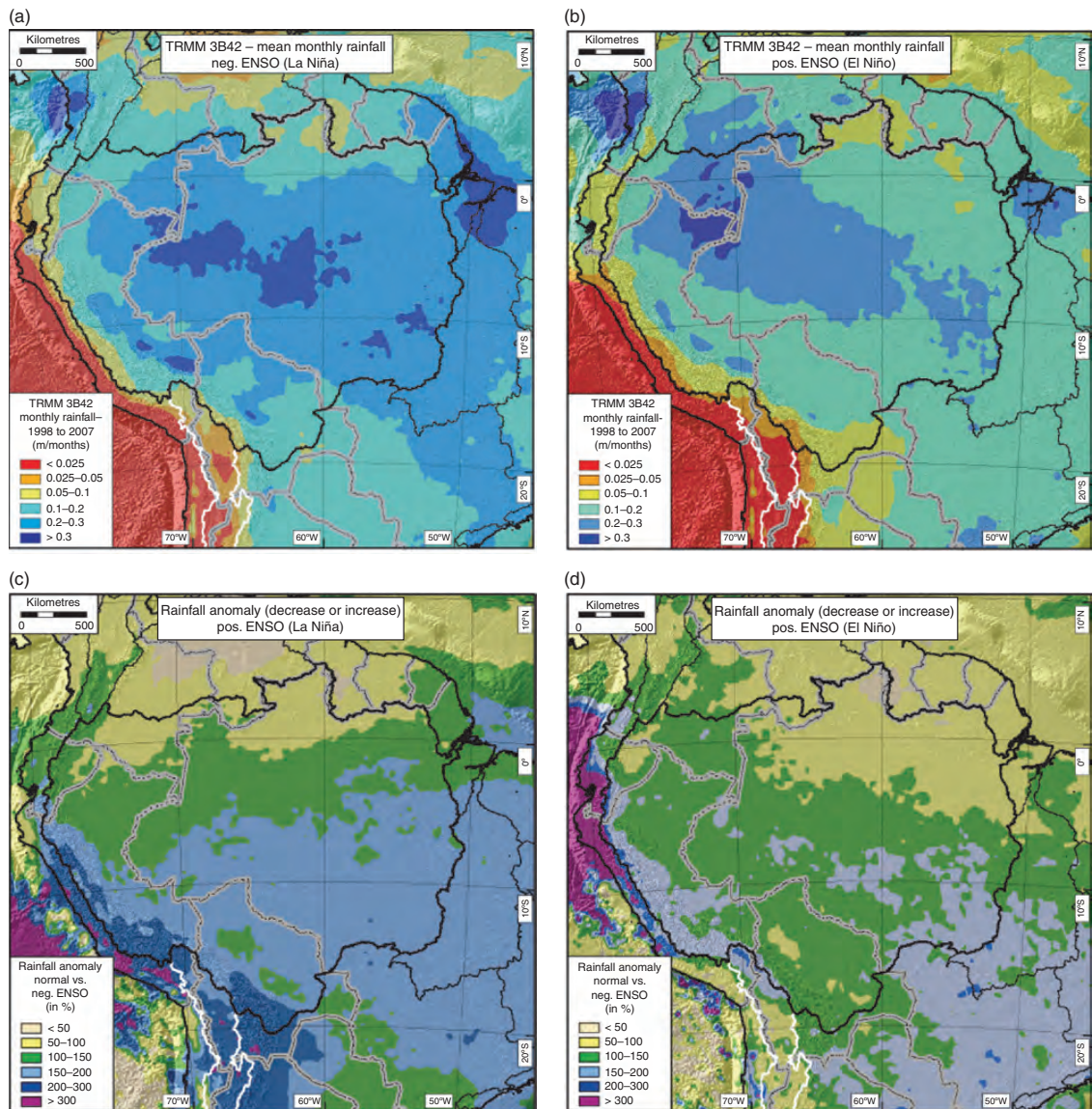
Plate 5 El Niño-Southern Oscillation (ENSO) rainfall maps (see Chapter 14). **(a)** Mean monthly rainfall for all negative ENSO anomalies from 1998 as identified by the Bivariate ENSO Timeseries (BEST) index. Note the high rainfall amounts throughout the central and southern Amazon catchment sectors, including the eastern flanks of the Andes in Peru and Bolivia. **(b)** Mean monthly rainfall for all positive ENSO anomalies from 1998, as identified by the BEST index. Note the moderate to high rainfall amounts along the Pacific coast of Ecuador and Colombia. In general, the Amazon drainage basin receives lower amounts of rainfall during positive ENSO anomalies, although rainfall is highly disparate in space and time. **(c)** Rainfall anomaly between negative ENSO (La Niña) months and non-ENSO months. Rainfall is shown as percentage increase. For example, the green colours depict rainfall increase by a factor of 1–1.5 and light-blue colours indicate an increase by a factor of 1.5–2.0. Note the latitudinal zonation and large rainfall increase in the high-elevation sectors of the Andes and along their eastern flanks. **(d)** Same as in (c), but for positive ENSO (El Niño) months. Rainfall most dominantly increases on the western flanks of the Andes during positive ENSO events.